HHS Public Access

Author manuscript

Neurobiol Aging. Author manuscript; available in PMC 2018 January 01.

Published in final edited form as:

Neurobiol Aging. 2017 January ; 49: 165–182. doi:10.1016/j.neurobiolaging.2016.10.003.

Low-level laser therapy for beta amyloid toxicity in rat hippocampus

Yujiao Lu[a], **Ruimin Wang**[a,b,**], **Yan Dong**[a], **Donovan Tucker**[a], **Ningjun Zhao**[a], **Md Ejaz Ahmed**[a], **Ling Zhu**[c], **Timon Cheng-Yi Liu**[c], **Robert M. Cohen**[d], and **Quanguang Zhang**[a,*]

[a]Department of Neuroscience and Regenerative Medicine, Medical College of Georgia, Augusta University, Augusta, GA, USA

[b]Neurobiology Institute of Medical Research Center, North China University of Science and Technology, Tangshan, China

[c]Laboratory of Laser Sports Medicine, College of Physical Education and Sports Science, South China Normal University, Guangzhou, China

[d]Department of Psychiatry and Behavioral Sciences and Neuroscience Program, Emory University, Atlanta, GA, USA

Abstract

Beta amyloid (Aβ) is well accepted to play a central role in the pathogenesis of Alzheimer's disease (AD). The present work evaluated the therapeutic effects of low-level laser irradiation (LLI) on Aβ-induced neurotoxicity in rat hippocampus. Aβ 1–42 was injected bilaterally to the hippocampus CA1 region of adult male rats, and 2-minute daily LLI treatment was applied transcranially after Aβ injection for 5 consecutive days. LLI treatment suppressed Aβ-induced hippocampal neurodegeneration and long-term spatial and recognition memory impairments. Molecular studies revealed that LLI treatment: (1) restored mitochondrial dynamics, by altering fission and fusion protein levels thereby suppressing Aβ-induced extensive fragmentation; (2) suppressed Aβ-induced collapse of mitochondrial membrane potential; (3) reduced oxidized mitochondrial DNA and excessive mitophagy; (4) facilitated mitochondrial homeostasis via modulation of the Bcl-2-associated X protein/B-cell lymphoma 2 ratio and of mitochondrial anti-oxidant expression; (5) promoted cytochrome c oxidase activity and adenosine triphosphate synthesis; (6) suppressed Aβ-induced glucose-6-phosphate dehydrogenase and nicotinamide adenine dinucleotide phosphate oxidase activity; (7) enhanced the total antioxidant capacity of hippocampal CA1 neurons, whereas reduced the oxidative damage; and (8) suppressed Aβ-induced reactive gliosis, inflammation, and tau hyperphosphorylation. Although development of AD treatments has focused on reducing cerebral Aβ levels, by the time the clinical diagnosis of AD or mild cognitive impairment is made, the brain is likely to have already been exposed to years

*Corresponding author at: Department of Neuroscience and Regenerative Medicine, Medical College of Georgia, Augusta University, 1120 15th Street, Augusta, GA 30912, USA. Tel.: (706) 446-4283; fax: (706) 721-8685. qzhang@gru.edu (Q. Zhang).

**Corresponding author at: Department of Neuroscience and Regenerative Medicine, Medical College of Georgia, Augusta University, 1120 15th Street, CA 3050, Augusta, GA 30912, USA. Tel.: (706) 721-7025; fax: (706) 721-8685. minruiwang@gmail.com (R. Wang).

Disclosure statement

The authors have no conflicts of interest to disclose.

of elevated Aβ levels with dire consequences for multiple cellular pathways. By alleviating a broad spectrum of Aβ-induced pathology that includes mitochondrial dysfunction, oxidative stress, neuroinflammation, neuronal apoptosis, and tau pathology, LLI could represent a new promising therapeutic strategy for AD.

Keywords

Alzheimer's disease; Low-level laser therapy; Mitochondrial dysfunction; Inflammation; Cognition

1. Introduction

As the world's most common form of dementia among elderly individuals, Alzheimer's disease (AD) causes neuronal degeneration, resulting in cognitive deficits and impaired behaviors (Serrano-Pozo et al., 2011). Characterized by extracellular β-amyloid plaque (in particular formed by Aβ 1–42 peptide) and neurofibrillary tangles within neurons, the vast majority of drug development for the treatment of AD has been based on the hypothesis that it is an excess of cerebral Aβ that triggers a cascade of events that include mitochondrial dysfunction, oxidative stress, and neuroinflammation that lead to neuronal dysfunction and ultimately neuronal death (Behl and Holsboer, 1998; Cadonic et al., 2015; Griffin and Mrak, 2002; Heneka and O'Banion, 2007; Simonian and Coyle, 1996).

Critically important for cell survival, mitochondria are the primary source of cellular energy generation. Mitochondria are highly dynamic with morphology and number regulated by the balance between fission and fusion proteins (Itoh et al., 2013). Aberrant mitochondrial fragmentation resulting from imbalance in the fusion-fission process leading to impaired mitochondrial function and neuronal death, are pathological findings in many neurodegenerative disorders including AD (Cadonic et al., 2015), and may represent a seminal event in the pathway leading to neurodegeneration. In line with this concept, compelling studies have pointed to the negative alterations of mitochondrial function at early stages of AD, including mitochondrial dynamic imbalance mediated by elevated ratios of fission over fusion proteins, massive megapore formation, enhanced autophagy activity, reduced anti-oxidant capacity, and failed adenosine triphosphate (ATP) production (Burte et al., 2015; Cabezas-Opazo et al., 2015; Grimm et al., 2016). Therefore, maintaining a healthy mitochondrial dynamics by balancing the fusion-fission process may sustain mitochondrial function and promote neuronal survival in neurodegenerative disease.

The progression of AD is also characterized by activation of microglia and reactive astrogliosis. Reactive gliosis contributes to local inflammation and oxidative stress resulting in changes in neuronal microenvironment, which further contributes to mitochondrial dysfunction and neuronal damage (Moreira et al., 2009, 2010; Steardo et al., 2015; Verkhratsky et al., 2016; von Bernhardi et al., 2015). Furthermore, previous work by our laboratory and others demonstrates that excessive superoxide anion derived from dysfunctional mitochondria and nicotinamide adenine dinucleotide phosphate (NADPH) oxidase plays pivotal roles in Aβ-induced neurofibrillary tangles, oxidative damage, and functional deficits (Block, 2008; Choi et al., 2012; Keller et al., 1998; Zhang et al., 2009,

2013). Another critical process associated with neuronal degeneration in AD, neuroinflammation, is mainly mediated by activated microglia and astrocytes that secrete a wide spectrum of proinflammatory cytokines, further aggravating Aβ neurotoxicity and causing consequent neuronal damage. Studies also show that proinflammatory cytokines are associated with neuronal degeneration in AD patients (Boissiere et al., 1997; Zhang and Jiang, 2015). Moreover, neuroinfiammation plays a critical role in Aβ-induced hippocampal neurotoxicity and memory impairment in animal models (He et al., 2011; Ryu et al., 2004; Sachdeva and Chopra, 2015), making neuroinfiammation a valuable research target for preclinical study of potential AD treatments.

Currently, FDA-approved drug treatments for AD at best induce some temporary improvements in cognitive and behavioral signs and symptoms in selective patients. Unfortunately, the vast majority of patients benefit only from a temporary halt or slowing of progression of their symptoms with no apparent effect on the underlying pathology. LLI is an emerging therapeutic technology that has recently been applied to several models of neurodegenerative disorders. LLI uses near infrared light to stimulate cytochrome c oxidase (CCO) in the mitochondria, relying on the gap in the absorption spectra of between water and biological chromophores to deliver low energy, nonheating infrared light deeply into tissues of interest (Abe et al., 1995; Chung et al., 2012). By increasing the activity of CCO in establishing the mitochondrial transmembrane proton gradient, ATP synthase activity increases, and net ATP production is consequently elevated (Karu et al., 1995; Pastore et al., 1994). Furthermore, LLI can also result in the release of bound nitric oxide from CCO (Karu et al., 2005). These effects in combination lead to a range of effects, including increased ATP content (Karu et al., 1995), altered mitochondrial dynamics (Pastore et al., 1994), apparent vasodilation (Plass et al., 2012), and inflammation mitigation (Muili et al., 2012). LLI has shown beneficial effects in models of stroke (Huisa et al., 2013), traumatic brain injury (Xuan et al., 2014), and Parkinson’s disease (Ying et al., 2008) by ameliorating neuronal damage and improving behavioral outcomes. Likewise, our recent study also demonstrated the remarkable action of LLI to attenuate depression-like behaviors and related ATP biosynthesis decline by facilitating mitochondrial CCO activity in the prefrontal cortex (Xu et al., 2016). Intriguingly, recent studies of Aβ-induced cell injury have suggested a potential role for LLI in the treatment of neurodegenerative disease (Farfara et al., 2015; Johnstone et al., 2015; Meng et al., 2013; Song et al., 2012). Particularly, a previous in vitro study involving LLI on Aβ-treated mouse hippocampal neurons displayed a robust increase in brain-derived neurotrophic factor expression and strong amelioration in dendritic atrophy (Meng et al., 2013). However, associated in vivo studies involving LLI improvement on AD are still insufficient, and the underlying molecular mechanisms responsible for LLI’s efficacy have not yet been elucidated, which is the focus of the present study.

2. Materials and methods

2.1. Experimental design and drug administration

Male Sprague Dawley rats (250–280 g, Charles River Laboratories) were randomly divided into 5 groups: (1) healthy animals that received hippocampal vehicle infusions (HC or

control); (2) healthy animals that received LLI (HC-LLI); (3) animals that received Aβ (1–42) infusions plus sham LLI (Aβ-SHAM); (4) animals that received hippocampal Aβ (1–42) infusions plus LLI (Aβ-LLI); and (5) animals that received hippocampal scrambled Aβ (1–42) infusions (Scr-Aβ). All procedures were approved by the Animal Care and Use Committees (Protocol #2014-0661) for care and use of animals and were in accordance with National Institutes of Health guidelines. The detailed experimental design for the studies is presented in Fig. 1A. Intrahippocampal injection of Aβ was carried as described in our previous study (Zhang et al., 2013). Briefly, full-length Aβ (1–42) or scrambled Aβ (1–42) (AnaSpec Inc, Fremont, CA, USA) was dissolved in 35% acetonitrile solution, diluted to a concentration of 500 μM with 0.1-M sterile-filtered phosphate buffered saline (PBS), and incubated for 18 hours at 37 °C. For hippocampal infusions of Aβ peptide, rats were anesthetized with sodium pentobarbital (50 mg/kg, intraperitoneal injection [i.p.]) and mounted in a stereotaxic apparatus. Aβ (1–42; 1 nmol in 2 μL), scrambled Aβ (1–42; 1 nmol in 2 μL) or vehicle (2 μL) were infused bilaterally at a rate of 0.5 μL/min using a Hamilton microsyringe to the coordinates targeting the stratum radiatum of medial CA1 region (anterior/posterior: −3.6 mm, medial/lateral: ± 2.0 mm, and dorsal/ventral: −2.8 mm), as illustrated in Fig. 1B. The needle was left in situ for 5 minutes before retraction, and retracted over 2 minutes. The incision was closed using wound clips, and rats were placed on a warming pad to recover from anesthesia. The animals were sacrificed under deep anesthesia at different pathological stages, and the brains were collected for immunofluorescent staining, Western blot, and biochemical analyses. Behavioral tests for the functions of hippocampus were carried out 12–18 days after Aβ injection.

2.2. Low-level laser irradiation (LLI) treatment

A diode laser (Diode IR Laser System, 808M100, Dragon Lasers) with continuous wave (CW) at 808 nm was used transcranially by focusing the beam (1 cm^2 round spot, centered at 3 mm posterior to the eye and 2 mm anterior to the ear) from the fiber optic on the top of the rat head with shaved scalp (see schematic diagram in Fig. 1C). Two-minute daily LLI treatment was initiated 3 hours after Aβ injection for 5 consecutive days (Fig. 1A). LLI-untreated control animals with Aβ peptide infusion (Aβ-SHAM) underwent identical procedures except that the laser power was not turned on. All the Aβ-treated animals were transiently restrained in a transparent DecapiCone (DCL-120, Braintree Scientific, Inc, MA, USA) during sham treatment or LLI treatment and released to their cages immediately after LLI treatment. The laser power density propagated through the transparent bag/fresh scalp/skull used in this study was adjusted to 25 mW/cm^2 at cerebral cortex tissue level (without local temperature increase in the scalp and brain tissue). The power density received by hippocampus tissue was about 8.33 ± 0.27 mW/cm^2 (N = 6). Two laser power meters (#FM33-056, Coherent Inc, USA; and #LP1, Sanwa, Japan) were used to measure the power density. The dose each animal received was 15 J/cm^2 at the cerebral cortex tissue level (~5.0 J/cm^2 at hippocampus level, calculated by total irradiated time (second) × power output (mW/cm^2)/1000, expressed as J/cm^2). The optimal and effective doses of this diode laser source following Aβ (1–42) injection were confirmed in a preliminary study in our laboratory (surviving neurons on day 18 after Aβ infusion: 26.50 ± 1.77% at 1-dose LLI (3 J/cm^2), 41.17 ± 3.10% at 3-dose LLI (9 J/cm^2), 79.17 ± 5.10% at 5-dose (15 J/cm^2), and 77.50 ± 3.97% at 6-dose LLI (18 J/cm^2) compared to 27.59 ± 5.03% in LLI-untreated Aβ

control, also see Fig. 2), and ensured to be within the “safety margin”. An additional control group, consisting of healthy control animals without Aβ infusion that received LLI treatment, was also included in this study (N = 6). We were unable to identify any pathologic changes up to 60 days in healthy animals treated with LLI at the high dose of 84 J/cm^2 (2-minute daily treatment for 4 weeks). For the sake of brevity and clarity of presentation, no further details of the results obtained studying these additional control groups are given in this manuscript.

2.3. Histological analysis

Histological examination of the brain was performed with NeuN, F-Jade B, and terminal deoxynucleotidyl transferase dUTP nick end labeling (TUNEL) staining as previously described (Zhang et al., 2009). Animals 18 days after Aβ injection were anesthetized, and then transcardially perfused with PBS followed by 4% paraformaldehyde. Brains were removed, postfixed, and cryoprotected with 30% sucrose until they sank. Frozen sections (25 μm each) were cut on a Leica Rm2155 microtome in the coronal plane of the dorsal hippocampus (~2.5–4.5 mm posterior from Bregma, ~100 sections per brain). Every fifth section was saved in stock solution for required staining. Staining for NeuN and F-Jade B was performed using a mouse anti-NeuN monoclonal antibody (1:500; EMD Millipore) and F-Jade B (AG310; EMD Millipore). NeuN positive cells with intact and round nuclei and negatively stained with Fluoro-Jade B were counted as surviving cells. TUNEL staining was performed on free-floating coronal sections using the Click-iT Plus TUNEL assay kit (Thermo Fisher Scientific) according to the manufacturer’s instructions. Slides for negative control were incubated with the label solution without terminal transferase for TUNEL. All the images were captured on an LSM510 Meta confocal laser microscope (Carl Zeiss) as described previously (Zhang et al., 2013). For quantitative analyses, the number of F-Jade B, NeuN, and TUNEL-positive cells per 250-μm length of medial CA1 region was counted bilaterally in 3–5 representative sections per animal. Cell counts from the right and left hippocampus were averaged to provide a single value for each animal. A means ± standard error (SE) was calculated from the data in each group (n = 5–8). Statistical analysis was performed as previously described.

2.4. Brain homogenates and subcellular fractionation

Animals were sacrificed by decapitation under deep anesthesia 6 days after hippocampal injection of Aβ peptide, and brains were rapidly removed. Hippocampal CA1 regions were quickly micro-dissected from both sides of the hippocampal fissures on an ice pad using a standardized microdissection procedure. The separated tissues were immediately frozen in liquid nitrogen until use. Total protein fractions, mitochondrial fractions, and cytosolic fractions were prepared as previously described (Han et al., 2015), using a motor-driven Teflon homogenizer in 1-mL ice-cold homogenization buffer (50-mM 4-(2-hydroxyethyl)-1-piper-azineethanesulfonic acid [HEPES], pH 7.4, 150-mM NaCl, 12-mM β-glycerophosphate, 1% Triton X-100) with inhibitors of proteases and enzymes (Thermo Scientific, Rockford, IL, USA). The homogenates were vigorously mixed for 20 minutes on a rotator and centrifuged at 15,000 × *g* for 30 minutes at 4 °C to obtain total protein fractions in the supernatants. For subcellular fractionation, tissues were homogenized in ice-cold buffer containing 10-mM HEPES (pH 7.9), 12-mM β-glycerophosphate, and inhibitors of

proteases and enzymes. After the addition of NP-40 to 0.6%, the homogenates were allowed to sit on ice for 10 minutes and vigorously vortexed for 30 seconds. The homogenates were then centrifuged at 800×*g* at 4 °C for 10 minutes, and the pellets were discarded. The resulting supernatants were further centrifuged at 17,000 ×*g* for 20 minutes at 4 °C to yield crude mitochondrial fractions in the pellets and cytosolic fractions in the supernatants. Protein concentrations were determined via Modified Lowry Protein Assay (Pierce, Rockford, IL, USA).

2.5. Western blotting and co-immunoprecipitation

Western blotting and co-immunoprecipitation (Co-IP) was performed as described in detail previously by our laboratory (Han et al., 2015; Zhang et al., 2009). Proteins were transferred to poly-vinylidene difluoride membrane, blocked and incubated with primary antibody at 4 °C overnight. The membrane was then washed followed by incubation with HRP-conjugated secondary antibodies for 1 hour at room temperature. Bound proteins were visualized using a CCD digital imaging system (HM3050A, Zhanglab), and semi-quantitative analyses of the bands were performed with the ImageJ analysis software (Version 1.49; NIH, USA). Band densities for the indicated proteins were normalized to loading controls (COX4, GADPH, or β-Actin). A means ± SE was calculated from the data for graphical presentation and statistical comparison. Primary antibody sources were as follows: Phosphor-Drp1 S616 and S637 from Cell Signaling Technology; Drp1 and OPA1 from BD Biosciences; Antibodies against Mff, COX4, Mief, Fis1, Mfn1, B-cell lymphoma 2 (Bcl-2), Prx2, LC3B, Vimentin, and β-Actin from Proteintech Group, Inc; MAP2, active Bcl-2-associated X protein (Bax) (6A7), Cytochrome c and SOD2 from Santa Cruz Biotechnology, and PHF1 from Thermo Fisher Scientific. For Co-IP, 200-μg protein samples from mitochondrial fractions were incubated with 5-μg anti-Drp1 antibodies overnight. After the addition of protein A/G-Sepharose (Santa Cruz Biotechnology), the mixture was incubated at 4 °C for an additional 2 hours. The beads were isolated by centrifugation and washed 3 times with HEPES buffer and eluted by heating at 100 °C in Laemmli buffer. The associated proteins in immunoprecipitates were examined by Western blotting analysis with anti-Fis1 or anti-Mff antibody. The blot was also reprobed with anti-Drp1 antibody to confirm the successfully immunoprecipitated Drp1 protein.

2.6. Immunofluorescence staining and confocal microscopy

Immunofluorescence staining was performed as previously described (Zhang et al., 2009). Briefly, sections were incubated with 10% normal donkey serum for 1 hour at room temperature in PBS containing 0.1% Triton X-100, followed by incubation with appropriate primary antibodies overnight. The following primary antibodies were used: anti-NeuN (MAB377, Millipore); anti-MAP2 and Nitrotyrosine (3-NT) (Santa Cruz); anti-TOM20, Mff, Mief, MFN1, and ionized calcium-binding adapter molecule 1 (Iba1) (Proteintech Group); anti-4-HNE and 8-OHDG from Abcam Inc; anti-Cleaved Caspase-3/9, glial fibrillary acidic protein (GFAP), and Phospho-Histone H2A.X Ser139 (Cell Signaling); and anti-PHF1 (Thermo Fisher). Sections were then washed 4 times at room temperature, followed by incubation with proper Alexa Fluor 594/647/488 donkey anti-mouse/rabbit/goat secondary antibody (Thermo Fisher Scientific) for 1 hour at room temperature. After washes, sections were mounted and coverslipped in Vectashield mounting medium with 4′,

6-diamidino-2-phenylindole (H-1200; Vector Laboratories, Inc, CA, USA). To measure the depolarization of mitochondrial membrane potential (MMP), Mitotracker Red Staining was performed as described in our recent work (Lu et al., 2016). In brief, MitoTracker Red CMXRos (50 ng/mL in 100 μL of saline, Life Technologies) was administered intravenously via tail vein injection. Five minutes after injection, the animals were deeply anesthetized with isoflurane and perfused transcardially followed by paraformaldehyde fixation as previously described. Brain sections were collected and washed for 4 × 10 minutes by 0.1% PBS-Triton X-100 and briefly with distilled water. The sections were then mounted and coverslipped in Vecta-shield mounting medium with 4′,6-diamidino-2-phenylindole. All the fluorescence images were captured on an LSM510 Meta confocal laser microscope (Carl Zeiss) using either a 5× or 40–100× oil immersion Neofluor objective with the image size set at 1024 × 1024 pixels. The captured images were viewed and analyzed using LSM510 Meta imaging software. At least 4–5 representative sections per animal were used for immunostaining, and typical staining section was selected for presentation.

2.7. Duolink II proximity ligation assay

Duo-Link II in situ proximity ligation assay (PLA) immunoassay was performed as described in the recent studies (Sareddy et al., 2015; Tu et al., 2015). In brief, hippocampal tissue sections were blocked in 10% donkey serum for 1 hour and incubated overnight with appropriate primary antibodies at 4 °C. The slides were then incubated with Duolink PLA Rabbit MINUS and PLA Mouse PLUS proximity probes for 1 hour at 37 °C. Ligation and amplification were carried out using the Duolink in situ detection reagent kit (Sigma–Aldrich) according to the manufacturer's protocol. Images were captured under LSM510 confocal microscope, and red spots representing the interactions were quantitatively analyzed using NIH ImageJ software.

2.8. Quantification of ATP levels and cytochrome c oxidase activity

ATP concentration was determined using a kit of ENLITEN rLuciferase/Luciferin reagent (FF2021, Promega, Madison, WI, USA) as described (Lu et al., 2016). Briefly, 30 μg of sample proteins from total protein fractions were suspended in 100 μL of reconstituted rL/L reagent buffer containing luciferase, D-luciferin, Tris-acetate buffer (pH 7.75), EDTA, magnesium acetate, bovine serum albumin, and dithiothreitol. Light emission at 10-second intervals from the reaction was measured in a standard microplate luminometer (PE Applied Biosystems). Relative light units from "background blank" containing rL/L reagent and the homogenization buffer used to prepare the samples were subtracted from the sample light output in the assay. Values of ATP activity levels were determined using an ATP standard curve. CCO activity in the mitochondrial fractions was assessed using an activity assay kit (ab109911, Abcam Inc) according to the instruction of the manufacturer. CCO enzyme was immunocaptured within the 96-well microplate, and activity was determined colorimetrically by measuring the oxidation of reduced cytochrome c at 550 nm absorbance (Bio-Rad Benchmark Plus, Microplate Spectrophotometer). The data of ATP levels and relative CCO activity were quantified as percentage changes versus control group for graphical depiction.

2.9. Measurement of Aβ (1–42) levels

As described previously, a 2-step extraction method was used to measure Aβ peptides levels (Cohen et al., 2013). Briefly, detergent-soluble Aβ (1–42) was detected in protein samples prepared with homogenization buffer as previously described. Detergent-insoluble Aβ (1–42) levels were detected by extraction of homogenate pellets in the chaotropic agent, 5-M guanidine-HCl. Protein levels were normalized by Modified Lowry Protein Assay (Pierce, Rockford, IL, USA). Aβ species in 40-μg protein samples of the detergent-soluble and -insoluble fractions were quantified using an amyloid beta 42 enzyme-linked immunosorbent assay (ELISA) Kit (Catalog # KMB3441, ThermoFisher Scientific) in accordance with the manufacturer's instruction.

2.10. Measurement of glucose-6-phosphate dehydrogenase (G6PDH) activity and NADPH level

G6PDH enzyme activity in total protein fractions was detected in a 96-well microplate using an assay kit (MAK015, Sigma–Aldrich) according to the manufacturer's instructions. Briefly, 30 μg of sample proteins were suspended in 50 μL/well of master reaction mix. The oxidation absorbance of G6PDH generating nicotinamide adenine dinucleotide was measured every 5 minutes on a spectrophotometer (Bio-Rad) at 450 nm. Values of G6PDH activity levels were determined using a standard curve of nicotinamide adenine dinucleotide and expressed as percentage changes versus control group. Total NADPH level was measured in the whole-cell homogenates using a colorimetric NADPH assay kit (ab186033, Abcam Inc) in accordance with the instructions for use. Each sample was incubated with NADPH probe, and the NADP/NADPH recycling enzyme mixture for 15 minutes to 2 hours at room temperature, and absorbance values of NADPH probe were measured colorimetrically at 460 nm using a standard curve of NADPH. Total NADPH levels were then quantified as percentage changes versus control group for graphical presentation.

2.11. NADPH oxidase activity and superoxide production assay

NADPH oxidase activity and superoxide production were determined as described previously by the author (Zhang et al., 2009). Photon emission from the lucigenin-chemiluminescent reaction was measured by a standard luminometer (PE Applied Biosystems). NADPH oxidase activity was calculated as relative light unit changes per micrograms of protein. Superoxide production of the individual samples was carried out using the procedure described in the LumiMax Superoxide Anion Detection kit (Stratagene, La Jolla, CA, USA). A means ± SE was calculated from the data collected in each group for graphical depiction and was expressed as percentage changes versus control group.

2.12. Total antioxidant capacity assay

An antioxidant assay kit (709001, Cayman Chemical) was used to measure the total antioxidant capacity according to the vendor's instructions. The assay relies on the ability of antioxidants in the sample to inhibit the oxidation of 2,2′-azino-di-[3-ethylbenzthiazoline sulphonate] (ABTS) by metmyoglobin. The capacity of the antioxidants in the sample to prevent ABTS oxidation is compared with that of trolox. In brief, 10 μL of prediluted protein samples or trolox standards were added to 10 μL of metmyoglobin and 150 μL of

chromogen (ABTS) in the designated wells on the plate. The reactions were initiated by adding 40 μL of hydrogen peroxide working solution to each well. The plates were covered and incubated on a shaker for 5 minutes and read at 750 nm using a spectrophotometer (Bio-Rad). The average absorbance of standards was plotted as a function of the final trolox concentration (mM) according to the assay protocol. Total antioxidant capacities of the samples were calculated using the standard curve. Each sample was analyzed in triplicate, and the results were reported as percentage changes versus control group.

2.13. Proinflammatory cytokines assay

Levels of proinflammatory cytokines in each group were quantitatively detected by the indirect ELISA technique (Gan and Patel, 2013). Briefly, samples were diluted to 50 μL containing the same amount of proteins using bicarbonate/carbonate coating buffer (Sigma–Aldrich). The dilutions were then loaded in polyvinyl chloride ELISA microplate (Corning), sealed and incubated overnight at 4 °C. The plate wells were washed 3 times, and the remaining protein-binding sites in the coated wells were blocked by adding 200-μL blocking buffer (1% bovine serum albumin in PBS, 0.3% solution of H_2O_2) for 1 hour at room temperature. Afterward, 50 μL of monospecific antibodies were added and incubated for 4 hours at 37 °C. The plate wells were then washed 3 times and incubated with HRP-conjugated secondary antibodies for 1 hour at room temperature, followed by another 3 times of washes. Finally, the plate was developed by incubating with 3,3′,5,5′-tetramethylbenzidine solution (Thermo fisher) for 30 minutes at room temperature, and reaction was stopped with 50 μL of sulfuric acid. The optical density was read at 450 nm on a spectrophotometer (Bio-Rad), and values were calculated and expressed as percentage changes versus control group.

2.14. Caspase activity assay

Caspase-3 and caspase-9 activities were measured in cytosolic protein fractions using fluorometric substrates as previously described by our laboratory (Lu et al., 2016). The substrates for caspase-3 and caspase-9 were Ac-DEVD-AMC and Ac-LEHD-AMC (AnaSpec, Fremont, CA, USA), respectively. The substrates were cleaved proteolytically by the corresponding caspases, and the fluorescence of free AMC was measured. Fluorescence was determined with an excitation wavelength of 360 nm and an emission wavelength of 460 nm for AMC, in a Synergy HT Microplate reader (BioTek Instruments Inc, Winooski, VT, USA). Values were expressed as changes in fluorescent units per microgram of protein and presented as percentage of control group.

2.15. Barnes maze task

The Barnes maze task, a widely accepted test of hippocampus-dependent spatial reference learning and memory in rats (Barnes et al., 1994; Cohen et al., 2013), was performed as described previously by our laboratory (Lu et al., 2016). The maze paradigm consists of a circular platform of 122 cm diameter elevated 1 m above the floor, with 18 holes around the perimeter and a recessed chamber (black escape box, 20 × 15 × 12 cm) located under one of the holes. Several visual cues were placed surrounding the maze to optimize cognitive performance. Testing was performed in a darkened room with bright flood incandescent light (500W, 1000 lux) shining down on the maze center. The behavior test was divided into

3 stages as follows: stage 1, trial tests on day 12, 13, and 14 after Aβ injection. During the 3-minute trials, the traces of rats from center of the platform to the escape chamber were recorded using an overhead video camera controlled by ANY-maze video tracking software (Stoelting Co, Wood Dale, IL, USA). After entering the escape box at the end of the trial, each rat was allowed 30 seconds in the escape chamber for habituation with the hole covered. Stage 2, probe test on day 15 after Aβ injection was carried out. In this stage, the escape chamber was removed, and the time spent in the target quadrant where the escape box had been was recorded during a 90-second period. Stage 3, probe test on day 18 after Aβ injection was carried out to test the long-term improvement of LLI on Aβ-induced spatial learning and memory. The platform was cleaned with 70% ethanol and dried with a blower fan after each test. The escape latency, escape velocity, and the time spent in the target quadrant (quadrant occupancy) were quantified afterward using ANY-maze software.

2.16. Novel object recognition (NOR)

NOR test was used to evaluate the effects of LLI on the functional improvement in recognition memory, a hippocampus-dependent working memory (Cohen et al., 2013; Wan et al., 1999). NOR test is based on the spontaneous tendency of rats to spend more time exploring a novel object than a familiar object. One day before test, the animals were allowed 5 minutes to explore the empty arena of the box (40 × 50 × 50 cm) for habituation. At day 17 after Aβ infusion, animal was placed in the object recognition box containing 2 identical objects fixed to the floor at an equal distance. After 5 minutes, the rat was removed from the object recognition box and returned to its home cage. Twenty-four hours later, the rats were returned to the object recognition box in the presence of one familiar object and a novel object to test long-term recognition memory. The novel object is generally consistent in height and volume with the familiar object but is different in shape and appearance. Exploration of the object was defined as the animal's nose being in the zone at a distance of less than 2 cm. The time spent exploring each object and the discrimination index percentage (the percentage time spent exploring the new object) was recorded and analyzed using ANY-maze video tracking software as previously mentioned.

2.17. Data analysis

Statistical analysis was performed using either 1-way or 2-way analysis of variance, followed by Student–Newman–Keuls posthoc tests to determine group differences. When groups were compared to the normal control group, Dunnett's test was adopted for posthoc analyses after analysis of variance. When only 2 groups were compared, a student t test was used. Statistical significance was accepted at the 95% confidence level ($p < 0.05$). Data were expressed as means ± SE.

3. Results

3.1. LLI suppressed Aβ-induced neuronal degeneration in hippocampual CA1 region

To investigate the effects of LLI on Aβ-induced early dendrite damage 6 days after Aβ administration, brain sections were labeled with MAP2, a sensitive and early indicator for the assessment of neuronal injury (Kitagawa et al., 1989). As shown in Fig. 2A and C, compared to controls (HC), Aβ (1–42) hippocampal infused rats (Aβ-SHAM) had less

MAP2 fluorescent staining intensity and greater MAP2 dispersion in the hippocampal CA1 stratum radiatum reflective of dendritic damage in the Aβ (1–42) hippocampal infused rats. In contrast, dendritic morphology was spared in Aβ (1–42) hippocampal infused rats that received LLI (Aβ-LLI) treatment. To explore the long-term effects of LLI on Aβ-induced neuronal degeneration, brain sections were stained with F-Jade B and NeuN 18 days after Aβ infusion. As shown in Fig. 2B and D, Aβ hippocampal infusion resulted in ~70% of neuronal loss and significant degeneration of pyramidal neurons in the CA1 region, which was significantly ameliorated by LLI treatment. To understand whether the neuroprotective effects of LLI were related to an effect on hippocampal Aβ levels, detergent-soluble and guanidine-soluble (detergent-insoluble) Aβ (1–42) were determined in hippocampal protein samples using an ELISA kit. Results indicated that the level of Aβ (1–42), at day 18 after Aβ (1–42) infusion, was not significantly affected following LLI treatment (detergent-soluble: 12.92 ± 2.16 pg in Aβ-LLI versus 11.70 ± 1.63 pg in Aβ-SHAM; guanidine-soluble: 5.37 ± 1.31 pg in Aβ-LLI versus 5.71 ± 1.44 pg in Aβ-SHAM; N = 6). In contrast to its effects in the CA1 region of the hippocampus, hippocampal CA1 infusion of Aβ (1–42) had no significant effects on neuronal degeneration over the time span of our study in other brain regions examined including cerebral cortex, hippocampal dentate gyrus, and CA3 subfields (data not shown). Moreover, neuronal degeneration (F-Jade B staining) and cell loss (NeuN staining) at day 18 were not observed in the hippocampal CA1 region of the healthy control animals that received 5 doses of LLI treatment at 15 J/cm^2 (HC-LLI).

3.2. LLI alternated mitochondrial targeting fission and fusion protein levels following Aβ insult

To examine the role of mitochondrial dynamics in Aβ-induced neurodegeneration and the potential protective effects of LLI treatment on Aβ (1–42) induced mitochondria damage, we next explored the effects of LLI on mitochondrial targeting fission proteins. Mitochondrial fractions from CA1 region were subjected to Western blotting and quantitative analyses. As shown in Fig. 3A–C, the levels of tested fission proteins Drp1, Fis1, Mff, and Mief were remarkably elevated in the Aβ (1–42)-treated group (Aβ-SHAM) compared with control group (HC), whereas LLI treatment significantly suppressed these elevations (Aβ-LLI vs. Aβ-SHAM). Corresponding triple-labeling confocal microscopy studies were successively carried out. Fig. 4A shows that Aβ hippocampal infusions promoted the mitochondrial localization of Drp1, Fis1, Mff, and Mief proteins (yellow). Note the increased expression of mitochondrial targeting fission-related proteins in Aβ (1–42) hippocampal infused animals (Aβ-SHAM vs. HC) were effectively suppressed by LLI (bottom panel: Aβ-SHAM vs. Aβ-LLI). It has been demonstrated that Drp1 activity is regulated by several posttranslational modifications, including phosphorylation of Drp1-S616 (required for mitochondrial fission) and Drp1-S637 (serves to suppress fission process) (Cereghetti et al., 2008; Cribbs and Strack, 2007). Interestingly, results in Fig. 3B revealed that Drp1-S616 level was higher and Drp1-S637 level was lower in Aβ-treated animals (Aβ-SHAM vs. HC) although all these differences were significantly reduced by LLI (Aβ-SHAM vs. Aβ-LLI). Because mitochondrial adaptor proteins for Drp1, Fis1, and Mff located in the outer mitochondrial membrane are involved in mitochondrial fission via binding to Drp1 (Palmer et al., 2013), Co-IPs were subsequently performed in mitochondrial protein samples with anti-Drp1 antibody and then separately blotted with anti-Fis1 or anti-

Mff antibody. As shown in Fig. 3D and E, the complex formations of Drp1-Fis1 and Drp1-Mff were markedly increased in Aβ-treated animals (Aβ-SHAM vs. HC) and significantly attenuated by LLI (Aβ-SHAM vs. Aβ-LLI). The protein-protein interactions were further analyzed by Duo-Link II in situ PLA immunoassay 6 days after Aβ infusion. Fig 3F shows representative confocal microscopy images of Drp1-Fis1/Mff interactions with Fig. 3G a bar graph of the quantitative analyses of the spots density representing the Drp1-Fis1/Mff interactions illustrating the statistically significantly higher interactions resulting from Aβ (1–42) infusion (Aβ-SHAM vs. HC) and the effectiveness of LLI in regulating mitochondrial fission (Aβ-SHAM vs. Aβ-LLI). In addition, OPA1 and MFN1, key fusion proteins and regulators of mitochondrial dynamics were analyzed by Western blotting and triple-labeled confocal microscopy. As shown in Fig. 4B and C, mitochondrial expressions and localizations of OPA1 and MFN1 were drastically decreased in Aβ-treated animals compared with control animals (Aβ-SHAM vs. HC), whereas the decreases were remarkably attenuated following LLI (Aβ-SHAM vs. Aβ-LLI). These results demonstrate the effectiveness of LLI in preserving mitochondrial fusion proteins and promoting mitochondrial fusion while suppressing abnormally elevated mitochodrial fission.

3.3. LLI recovered Aβ-induced changes in mitochondrial dynamics in hippocampal CA1 neurons

We next investigated the effect of LLI on mitochondrial morphology following Aβ insult. As shown in Fig. 5A(a–c), representative confocal microscopy images show that mitochondria in the CA1 pyramidal neurons remain extensively fragmented 6 days following Aβ insult. For clear image views and quantitative analyses, acquired images of Tom20 fluorescent staining were thresholded, filtered, and binarized, using ImageJ software. As shown in Fig. 5A(a–i) and B (a and b), quantification of mitochondrial segments using the parameters for mitochondrial total particles and small particles (size <1.5 μm) revealed a markedly higher degree of mitochondrial fragmentation in Aβ-treated group than that in control group (Aβ-SHAM vs. HC). By contrast, the degree of Aβ-induced mitochondrial fragmentation was dramatically attenuated by LLI to a level comparable with control (Aβ-SHAM vs. Aβ-LLI). To add further support for LLI's ameliorating effect on Aβ-induced mitochondria fragmentation, continuous mitochondrial structures (size >2 μm) were analyzed. As indicated in Fig. 5A(a–c, i and j) and B (c), quantitative analyses demonstrated a significant recovery in the density of continuous mitochondrial structures in Aβ-LLI animals compared to Aβ-SHAM animals. Of importance, mitochondrial fragmentation was not significantly changed following a 5-dose LLI treatment of healthy animals (33.59 ± 3.10 in HC-LLI group vs. 32.17 ± 3.12 in HC, N = 6), as examined 18 days following initiation of LLI. These results suggest the important capability of LLI in balancing the opposing processes of mitochondrial fission and fusion during Aβ neurotoxicity while not adversely affecting mitochondrial fission and fusion in healthy tissue.

3.4. LLI suppressed Aβ-induced mitochondrial dysfunction in hippocampal CA1 neurons

Mitochondrial dysfunction resulting from deleterious fragmentation is an early and causal event in neurodegeneration (Knott et al., 2008). Mitochondrial degradation by autophagy (mitophagy) plays an important role in turnover of dysfunctional mitochondria, which has been implicated in the progression of AD (Baloyannis, 2006; Kim et al., 2007). We

measured mitophagy in mitochondrial fractions by monitoring the expression level of LC3B protein, a well-known marker of autophagy. Findings of increased levels of LC3B in Aβ (1–42) injected animals compared with controls (Aβ-LLI vs. HC) as well as LLI-treated Aβ infused animals (Aβ-LLI vs. Aβ-SHAM) suggest that LLI treatment has a salutary effect on Aβ-induced mitophagy (Fig. 6A). Consistent with this interpretation, LLI-untreated Aβ (1–42)-injected rats exhibited a high Bax/Bcl-2 ratio compared to controls (Aβ-SHAM vs. HC) and LLI-treated Aβ-infused animals exhibited a relatively preserved Bax/Bcl2 ratio (Aβ-SHAM vs. Aβ-LLI) comparable with healthy controls (Fig. 6B). In addition, the levels of mitochondrial targeting SOD2 and Prx2 were downregulated in Aβ (1–42) injected animals, whereas LLI facilitated their recoveries as shown in Fig. 6C.

To evaluate the effect of LLI on mitochondrial membrane integrity, MMP was assessed using MitoTracker Red fluorescent dye and confocal microscopy. Quantitative evaluation of MitoRed fluorescent intensities showed markedly decreased normalized fluorescent signals in CA1 pyramidal neurons 6 days after Aβ (1–42) injection in sham-treated animals (Aβ-SHAM vs. HC) but was not observed in Aβ (1–42) injected animals that had LLI (Aβ-LLI vs. HC), suggesting Aβ-induced mitochondrial depolarization, collapse of MMP that was prevented by LLI (Fig. 6D [C and d]). Oxidized mitochondrial DNA (mtDNA) was then evaluated by double labeling for 8-OHDG and TOM20 as shown in the representative images (Fig. 6E). Mitochondial oxidation was found to be substantially greater in Aβ-infused animals (Aβ-SHAM vs. HC) with the deleterious effects of Aβ infusion ameliorated with LLI (Aβ-SHAM vs. Aβ-LLI). Finally, CCO activity and levels of ATP production were measured using mitochondrial and total protein fraction samples, respectively. As shown in Fig. 6F and G, infusion of Aβ resulted in significant CCO activity decline and ATP depletion compared with those in control animals (Aβ-SHAM vs. HC) with animals treated with LLI being spared (Aβ-SHAM vs. Aβ-LLI). Taken together, these results clearly suggest that (1) Aβ-induced excessive mitochondrial fragmentation is associated with excessive mitophagy, mtDNA damage, and mitochondrial dysfunction; and (2) LLI is able to ameliorate Aβ (1–42) toxic effects on mitochondrial membrane integrity and function.

3.5. LLI inhibited Aβ-induced G6PDH and NADPH oxidase activities and oxidative damage; and enhanced total antioxidant capacity

There is accumulating evidence showing that mitochondrial dysfunction and oxidative stress are intimately involved in the early pathology of AD (Moreira et al., 2009, 2010). Previous work by our laboratory and others has demonstrated that excessive superoxide anion derived from NADPH oxidase and dysfunctional mitochondria play pivotal roles in oxidative neuronal damage (Choi et al., 2012; Keller et al., 1998; Zhang et al., 2009). We initially measured the changes of NADPH oxidase activity using CA1 proteins 6 days after Aβ infusion. Of significant interest, we found Aβ induced a remarkable increase of NADPH oxidase activity that could be effectively attenuated by LLI treatment (Fig. 7C) (Aβ-SHAM vs. HC; Aβ-SHAM vs. Aβ-LLI). Because G6PDH enzyme serves as a major source of NADPH in pentose phosphate pathway, which fuels NADPH Oxidase, we hypothesized that G6PDH could be involved in Aβ-mediated NADPH oxidase activation. Indeed, as shown in Fig. 7A and B, Aβ induced significant increases in G6PDH activity (Aβ-SHAM vs. HC) and NADPH generation (Aβ-SHAM vs. HC) 6 days after Aβ infusion compared to sham

control. In contrast, LLI treatment blocked the increases in G6PDH (Aβ-SHAM vs. Aβ-LLI) and NADPH activities (Aβ-SHAM vs. Aβ-LLI) as well as the increased level of NADPH (Aβ-SHAM vs. Aβ-LLI). Consistent with these novel findings, mitochondrial and cytoplasmic superoxide anion production from CA1 region protein samples was elevated in Aβ (1–42) infused animals (Aβ-SHAM vs. HC) with LLI-treated animals having significant protection (Aβ-SHAM vs. Aβ-LLI) (Fig. 7D). Consistent with the previous findings, mitochondrial and cytoplasmic total antioxidant capacity was significantly reduced in Aβ (1–42)-infused animals (Aβ-SHAM vs. HC), with LLI-treated animals maintaining total antioxidant capacity (Aβ-SHAM vs. Aβ-LLI) (Fig. 7E). In addition, as shown in Fig. 7F and G, confocal microscopy and fluorescent intensity examinations of oxidative damage markers were carried out on sections 6 days after Aβ infusion. The results revealed that, in agreement with reduction of superoxide anion by LLI, LLI markedly attenuated oxidative damage in CA1 neurons as measured by the oxidative damage markers for lipid peroxidation (4-HNE), peroxynitrite production (3-NT), DNA double-strand breaks (H2A.X Ser139), and oxidized DNA damage (8-OHdG). In summary, these findings imply that G6PDH-involved NADPH oxidase and dysfunctional mitochondria could be the major sources of oxidative stress that lead to oxidative neuronal damage following Aβ insult.

3.6. LLI suppressed Aβ-induced reactive gliosis, proinflammatory cytokines production, and tau hyperphosphorylation

We hypothesized that in addition to oxidative stress,glial activation could also be a consequence of Aβ-induced mitochondrial dysfunction, which in turn could contribute to inflammation and additional oxidative stress resulting in further neuronal damage. Western blotting analyses of Iba1 (a marker for microglia activation) and Vimentin (a marker for reactive astrocytosis) in total protein samples from CA1 region showed that Aβ (1–42) infusion caused significant increases in Iba1 (Aβ-SHAM vs. HC) and Vimentin (Aβ-SHAM vs. HC) levels compared with control groups 6 days after infusion (Fig. 8A). As shown in Fig. 8B–D, results from ELISA assays exhibited further findings of robust increases in the levels of proinflammatory cytokines interleukin-1 beta (IL-1β) (Aβ-SHAM vs. HC), interleukin-6 (Aβ-SHAM vs. HC), and tumor necrosis factor-alpha (Aβ-SHAM vs. HC) in Aβ (1–42) infused animals, providing additional support for Aβ (1–42) induced neuroinflammation. As expected, LLI significantly attenuated the elevation of glial activation and proinflammatory cytokine levels in the hippocampal CA1 region (Aβ-SHAM vs. Aβ-LLI). In addition, brain sections 18 days after Aβ injection were immunostained for detection of Iba1 and GFAP. Fig. 8E presents typical overview images of Iba1 (green) and GFAP (red) immunoreactivity showing remarkable activation of microglia and astrocytes in the hippocampal CA1 region. Fig. 8F shows representative confocal microscopy of enlarged Iba1 (green) and GFAP (red) staining taken from medial hippocampal CA1 region. Quantitative analyses show robust increases in immunoreactivity for Iba1 and GFAP in the Aβ-treated animals (Aβ-SHAM vs. HC) and decreases in LLI-treated animals (Aβ-SHAM vs. Aβ-LLI), respectively (Fig. 8F [j and k]). Additional studies revealed that Aβ also induced a robust hyperphosphorylation of the microtubule-associated tau protein in the CA1 region (Aβ-SHAM vs. HC) (Fig. 9A and B). The elevated levels of hyperphosphorylated tau (PHF1) protein were also effectively inhibited in the LLI-treated animals (Aβ-SHAM vs.

Aβ-LLI). Taken together, the results strongly support the LLI's efficacy in reducing Aβ (1–42) induced neuroinflammation and tau pathology.

3.7. LLI attenuates Aβ-induced cytosolic level of cytochrome c, caspase-9, and caspase-3 activities and neuronal apoptosis

Next, we investigated elements of the neuronal apoptotic pathway. First, the cytosolic distribution of Cyt *c* in response to Aβ insult was examined by Western blotting analyses. As shown in Fig. 10A, Aβ induced a significant elevation of cytosolic Cyt *c* content 6 days after Aβ (1–42) infusion compared with control group (Aβ-SHAM vs. HC), and the increase was attenuated by LLI treatment (Aβ-SHAM vs. Aβ-LLI). Subsequently, we found that LLI was effective in inhibiting Aβ-induced caspase-9 (Aβ-SHAM vs. HC; Aβ-SHAM vs. Aβ-LLI) and caspase-3 (Aβ-SHAM vs. HC; Aβ-SHAM vs. Aβ-LLI) activity in the CA1 region (Fig. 10B and C). Furthermore, immunostaining for active form of caspase-3 demonstrated a predominant activation of caspase-3 in CA1 neurons of Aβ-treated animal (Aβ-SHAM vs. HC), whereas caspase-3 activation was significantly reduced by LLI (Aβ-SHAM vs. Aβ-LLI) (Fig. 10D). These observations suggest the inhibitory effects of LLI on Aβ-mediated activation of caspase-9–dependent apoptotic pathway, and on the activation of caspase-3, a final executioner of apoptosis. Finally, apoptotic neuronal death in hippocampal CA1 was explored by TUNEL staining and cell-counting study. As presented in Fig. 10E, Aβ induced a robust increase in the number of TUNEL-positive cells compared with control (Aβ-SHAM vs. HC) and LLI-treated animal (Aβ-SHAM vs. Aβ-LLI), providing additional support for LLI's anti-apoptotic efficacy in the context of Aβ neurotoxicity.

3.8. LLI alleviated Aβ-induced behavioral deficits in Barnes maze task and novel object recognition test

To test whether LLI protection against Aβ (1–42) neurotoxicity extended to cognition, we assessed LLI-treated and sham-treated Aβ-infused animals as well as healthy controls on tests of spatial memory and object recognition. The Barnes maze is a widely accepted test of hippocampus-dependent spatial reference learning and memory (Barnes et al., 1994; Cohen et al., 2013), and the hippocampal CA1 region, in particular, plays a key role in processing topological spatial information (Goodrich-Hunsaker et al., 2008). As shown in Fig.11A and B, animals were subjected to training trials on days 12, 13, and 14 post Aβ infusion and probe trials performed on day 15 and day 18 post Aβ infusion. Animals treated with Aβ (1–42) were delayed in finding the black escape box on the last 2 days of training compared to control rats (Aβ-SHAM vs. HC) and LLI-treated Aβ-infused rats (Aβ-SHAM vs. Aβ-LLI; Fig. 11A–D). Importantly, escape velocity did not differ among the 3 groups, suggesting that differences were not due to variation in motoric abilities. In addition, Aβ-treated animals with LLI treatment and control animals spent significantly longer time in the target quadrant where the escape box had been located (Fig. 11B), compared with LLI-untreated Aβ group (Aβ-SHAM vs. HC and Aβ-SHAM vs. Aβ-LLI).

The novel object recognition test assesses hippocampus-dependent working memory in the rodent (Antunes and Biala, 2012; Leger et al., 2013). As shown in Fig. 11C, recognition memory was significantly impaired in animals 18 days after Aβ infusion, as indicated by comparison of the time spent exploring each object (Aβ-SHAM vs. HC) and the

discrimination index percentage (Aβ-SHAM vs. HC). Notably, Aβ-induced deficit in exploring novel object and the decrease in discrimination index were efficiently improved following LLI treatment, demonstrating the effectiveness of LLI in improving long-term learning and recognition memory (Fig. 11C). As an additional control, LLI was found to not have an effect on the cognition of animals that had not received Aβ (1–42) infusions. Specifically, quadrant occupancy on the probe trials of the Barnes maze test (HC-LLI: 84.20 ± 1.72; HC: 85.40 ± 1.40. N = 6, p = NS) and the discrimination test of the novel object recognition test (HC-LLI: 73.95 ± 1.85%; HC: 74.90 ± 1.16%, N = 6, p = NS), as examined on day 18 after 5-dose LLI treatment (15 J/cm2), showed no effect of LLI treatment.

4. Discussion

Aβ accumulation is believed to be the main cause of synaptic dysfunction and neuronal degeneration in the AD brain including the hippocampus, the region at the core of a cortical learning and memory system (Daulatzai, 2013; Fjell et al., 2014; Selkoe, 2004). Although the mechanism is yet unclear, AD progression and pathogenesis is widely accepted to be associated with a series of pathological events, initiated by neurotoxic levels of Aβ, that lead to intracellular neurofibrillary tangles, oxidative stress, neuro-inflammation, and mitochondrial dysfunction with consequent neuronal dysfunction and ending in cell death (Grimm et al., 2016; Qin et al., 2002; Serrano-Pozo et al., 2011; Zhang and Jiang, 2015). Using a rat model of hippocampal Aβ peptide injection, the present study demonstrated, for the first time, that LLI was able to attenuate Aβ-induced neurodegeneration and improve Aβ-induced impaired recognition memories. LLI had efficacious effects on mitochondrial homeostasis and dynamics, oxidative stress, neuroinflammation, and tau pathology without apparent effects when administered to healthy animals. Our results add to a growing body of evidence supportive of a pivotal role for mitochondrial dysfunction in AD pathogenesis.

It is likely that the deficient cellular energy production and extensive oxidative stress, the result of Aβ-induced mitochondrial dysfunction, are the initiators of the chain of events that lead to neuronal dysfunction, neurodegeneration, and memory impairments found in the present study. The mechanism of mitochondrial structure preservation has been widely reported to be associated with the balance of mitochondrial fission and fusion protein levels (Bertholet et al., 2016). Neurodegeneration is characterized by mitochondrial dysfunction and mitochondrial fragmentation. Following mitochondrial morphological changes, outer mitochondrial membrane per-meabilization occurs via the homo-oligomerization of Bax and Bak, and the formation of megapores allows the release of cytochrome c into the cytoplasm with consequent reduction in CCO activity (Galluzzi et al., 2009). The anti-apoptotic Bcl-2 protein prevents the homo-oligomerization of Bax and Bak, but Bcl-2 is downregulated in AD (Satou et al., 1995). In this study, Aβ injection into the hippocampus led to mitochondrial abnormalities including impaired mitochondrial dynamics and mitochondrial fragmentation. In contrast, LLI treatment was able to shift mitochondrial dynamics toward fusion by balancing the mitochondrial targeting fission proteins and fusion proteins. In addition, LLI treatment markedly reduced MMP collapse, oxidative mtDNA damage, and mitophagy proteins, supporting the ability of LLI to attenuate mitochondrial dysfunction and maintain mitochondria at a low level of mitophagy. Concomitantly, LLI modulated the mitochondrial targeting ratio of active Bax/Bcl-2 and antioxidant level, suggesting an

important role of LLI in facilitating mitochondrial homeostasis and protection in hippocampal CA1 neurons.

Impaired oxidative phosphorylation and reduced ATP levels are observed in the brains of AD patients (Pettegrew et al., 1994; Terni et al., 2010), suggesting that the AD brain is under energetic stress. Notably, the reduced mitochondrial enzyme activities and cerebral metabolism precede AD-associated neurological dysfunction as well as gross neuropathology (Sullivan and Brown, 2005). As the terminal protein complex and a key regulator in the mitochondrial electron transport chain, CCO is responsible for one of the final steps in oxidative phosphorylation (Ludwig et al., 2001). Both structurally abnormal CCO and reduced CCO activity were demonstrated in the brain of AD patients (Bosetti et al., 2002; Mutisya et al., 1994; Parker et al., 1990; Parker and Parks, 1995). In line with these findings, ATP synthase activity is also compromised in AD patients (Bosetti et al., 2002). Restored levels of CCO activity and ATP synthesis in LLI-treated animals with Aβ injection is of particular importance given the brain's dependence on aerobic metabolism. Although the precise underlying mechanism responsible for LLI modulation of mitochondrial function is unknown, the current findings are consistent with the positive effects of LLI on mitochondrial function that have been reported in a variety of in vitro and in vivo models (Chung et al., 2012; Farivar et al., 2014; Silveira et al., 2009; Souza et al., 2014).

It is becoming increasingly recognized that oxidative stress and neuroinflammation are strongly linked to mitochondrial dysfunction and to each other in AD pathology (De Felice and Ferreira, 2014; Freund-Levi et al., 2014; Urrutia et al., 2014; Wang et al., 2014; Witte et al., 2010). Oxidative stress causes a series of irreversible damages to biological systems by oxidizing all major biomolecules including nucleic acids, proteins, and lipids, with the brain particularly vulnerable (Wang et al., 2014). In the present study, LLI inhibited the Aβ-induced increase in G6PDH activity. This finding supports the likelihood that Aβ toxicity is the cause of the increased cerebral G6PDH activity found in AD brains (Martins et al., 1986). The increase in G6PDH activity would be expected to lead to NADPH accumulation by inhibiting aerobic glycolysis which in turn would be expected to lead to a shunting of glucose metabolism through the pentose phosphate pathway. Moreover, since NADPH fuels NADPH oxidase to generate superoxide anion, we hypothesized that G6PDH could be involved in Aβ-mediated NADPH oxidase activation. Indeed, increased NADPH generation and NADPH oxidase activity were observed to be increased following Aβ insult and diminished to basal control levels by LLL. These findings demonstrate the novel capability of LLI to attenuate oxidative damage by inhibiting G6PDH and NADPH oxidase activities, as well as limiting superoxide anion production.

Aβ injection into the hippocampus also led to a rapid inflammatory response. As major inflammatory mediators, activated microglia, and astrocytes secrete proinflammatory cytokines including IL-1β, interleukin-6, and tumor necrosis factor-alpha, paralleled by upregulation of nuclear transcription factors (McGeer and McGeer, 1995, 2001; Wilkins et al., 2015). Multifunctional proinflammatory cytokines induce a range of cellular responses that contribute together with dysfunctional mitochondria to regulate apoptosis via activation of caspase 3 and caspase 9. Consequent massive neuronal apoptosis can be observed

morphologically, accompanied by upregulation of autophagy proteins in the process of cellular degradation (Kraft and Kenworthy, 2012). Our current in vivo data demonstrate the efficacy of LLI on Aβ-induced reactive gliosis, inflammation, tau hyperphosphorylation, and neuronal apoptosis and extend earlier findings regarding the protective effects of LLI in suppressing Aβ-induced cellular injury in vitro (Bungart et al., 2014; Duan et al., 2003; Meng et al., 2013; Yang et al., 2010).

The vast majority of drug development for the treatment of AD has focused on reducing levels of brain amyloid. Although this strategy may prove effective prior to the onset of substantial amyloid accumulation, it now appears likely that by the time an individual develops symptoms of AD or mild cognitive impairment, the brain has already been exposed to years of excessive and presumably neurotoxic levels of Aβ. The consequence of such exposure is likely to be the impairment of multiple cellular pathways and the induction of neuroinflammation with dire consequences for the brain. As a result, treatments that selectively target production or elimination of Aβ, although effective in rodent models, are unlikely to be sufficient to reverse the further progression of the clinical disease.

It is important in this context to contrast this study with another recent study that investigated the ability of LLI to stimulate bone marrow (BM) in 5XFAD transgenic AD mouse model (Farfara et al., 2015). LLI to the BM was performed by placing the distal tip of the fiber optic on the tibia after making a small incision in the skin. They reported that weekly LLI to BM of AD mice for 2 months, starting at the progressive stage of AD, reduced Aβ burden in the brain and improved memory. Their data suggest the use of LLI as a therapeutic application in progressive stages of AD by the stimulation of autologous BM of AD mice. The present study suggests the utility of a novel broad spectrum approach as personified in the potent neuroprotective effect of LLI against Aβ neurotoxicity. Specifically, we used a different LLI protocol, that is, a noninvasive transcranial LLI treatment performed by simply applying the fiber optic directly on the top of the animal's head, initiated 3 hours after Aβ injection. Notably, the 5-day LLI does not block Aβ level in the hippocampus, but nevertheless did attenuate the toxic effects of Aβ, making it unlikely that the beneficial effects of LLI were due to elimination of Aβ. In emphasizing the contrasting strategies personified by these 2 studies of LLI, we are not ruling out the potential clinical benefit of combination therapies designed to lower amyloid levels while simultaneously providing neuroprotection.

The injection dose of Aβ (1 nmol) into brain tissue results considerable neuronal damage as early as 6–7 days after injection (Jantaratnotai et al., 2003; Ryu et al., 2004; Zhang et al., 2013), which supports the utility of testing memory deficits 12–18 days after Aβ infusion. It will be of interest in future studies to observe the effects of LLI on cognition months after Aβ infusion. Moreover, it will be important to identify the initiating physical basis of LLI's neuroprotective effect. Nevertheless, our findings suggest that the neuroprotection afforded by LLI is likely to be at least partially the result preservation of mitochondrial activity and integrity, oxidative stress suppression, and inflammatory response inhibition. These observations should encourage additional research on LLI as a treatment modality for AD.

Acknowledgments

This study was supported by research grant NS086929 from the National Institute of Neurological Disorders and Stroke, National Institutes of Health USA; an American Heart Association grant-in-aid 15GRNT25240004, and National Natural Science Foundation grants of China: 61575065 (to CYL), and 31171354 (to RMW).

References

Abe K, Aoki M, Kawagoe J, Yoshida T, Hattori A, Kogure K, Itoyama Y. Ischemic delayed neuronal death. A mitochondrial hypothesis Stroke. 1995; 26:1478–1489. [PubMed: 7631357]

Antunes M, Biala G. The novel object recognition memory: neurobiology, test procedure, and its modifications. Cogn Process. 2012; 13:93–110. [PubMed: 22160349]

Baloyannis SJ. Mitochondrial alterations in Alzheimer's disease. J Alzheimers Dis. 2006; 9:119–126. [PubMed: 16873959]

Barnes CA, Jung MW, McNaughton BL, Korol DL, Andreasson K, Worley PF. LTP saturation and spatial learning disruption: effects of task variables and saturation levels. J Neurosci. 1994; 14:5793–5806. [PubMed: 7931545]

Behl C, Holsboer F. Oxidative stress in the pathogenesis of Alzheimer's disease and antioxidant neuroprotection. Fortschr Neurol Psychiatr. 1998; 66:113–121. [PubMed: 9565761]

Bertholet AM, Delerue T, Millet AM, Moulis MF, David C, Daloyau M, Arnaune-Pelloquin L, Davezac N, Mils V, Miquel MC, Rojo M, Belenguer P. Mitochondrial fusion/fission dynamics in neurodegeneration and neuronal plasticity. Neurobiol Dis. 2016; 90:3–19. [PubMed: 26494254]

Block ML. NADPH oxidase as a therapeutic target in Alzheimer's disease. BMC Neurosci. 2008; 9(Suppl 2):S8. [PubMed: 19090996]

Boissiere F, Hunot S, Faucheux B, Duyckaerts C, Hauw JJ, Agid Y, Hirsch EC. Nuclear translocation of NF-kappaB in cholinergic neurons of patients with Alzheimer's disease. Neuroreport. 1997; 8:2849–2852. [PubMed: 9376517]

Bosetti F, Brizzi F, Barogi S, Mancuso M, Siciliano G, Tendi EA, Murri L, Rapoport SI, Solaini G. Cytochrome c oxidase and mitochondrial F1F0-ATPase (ATP synthase) activities in platelets and brain from patients with Alzheimer's disease. Neurobiol Aging. 2002; 23:371–376. [PubMed: 11959398]

Bungart BL, Dong L, Sobek D, Sun GY, Yao G, Lee JC. Nanoparticle-emitted light attenuates amyloid-beta-induced superoxide and inflammation in astrocytes. Nanomedicine. 2014; 10:15–17. [PubMed: 24200521]

Burte F, Carelli V, Chinnery PF, Yu-Wai-Man P. Disturbed mitochondrial dynamics and neurodegenerative disorders. Nat Rev Neurol. 2015; 11:11–24. [PubMed: 25486875]

Cabezas-Opazo FA, Vergara-Pulgar K, Perez MJ, Jara C, Osorio-Fuentealba C, Quintanilla RA. Mitochondrial dysfunction contributes to the pathogenesis of Alzheimer's disease. Oxid Med Cell Longev. 2015; 2015:509654. [PubMed: 26221414]

Cadonic C, Sabbir MG, Albensi BC. Mechanisms of mitochondrial dysfunction in Alzheimer's disease. Mol Neurobiol. 2015

Cereghetti GM, Stangherlin A, Martins de Brito O, Chang CR, Blackstone C, Bernardi P, Scorrano L. Dephosphorylation by calcineurin regulates translocation of Drp1 to mitochondria. Proc Natl Acad Sci U S A. 2008; 105:15803–15808. [PubMed: 18838687]

Choi DY, Lee YJ, Hong JT, Lee HJ. Antioxidant properties of natural polyphenols and their therapeutic potentials for Alzheimer's disease. Brain Res Bull. 2012; 87:144–153. [PubMed: 22155297]

Chung H, Dai T, Sharma SK, Huang YY, Carroll JD, Hamblin MR. The nuts and bolts of low-level laser (light) therapy. Ann Biomed Eng. 2012; 40:516–533. [PubMed: 22045511]

Cohen RM, Rezai-Zadeh K, Weitz TM, Rentsendorj A, Gate D, Spivak I, Bholat Y, Vasilevko V, Glabe CG, Breunig JJ, Rakic P, Davtyan H, Agadjanyan MG, Kepe V, Barrio JR, Bannykh S, Szekely CA, Pechnick RN, Town T. A transgenic Alzheimer rat with plaques, tau pathology, behavioral impairment, oligomeric abeta, and frank neuronal loss. J Neurosci. 2013; 33:6245–6256. [PubMed: 23575824]

Cribbs JT, Strack S. Reversible phosphorylation of Drp1 by cyclic AMP-dependent protein kinase and calcineurin regulates mitochondrial fission and cell death. EMBO Rep. 2007; 8:939–944. [PubMed: 17721437]

Daulatzai MA. Neurotoxic saboteurs: straws that break the hippo's (hippocampus) back drive cognitive impairment and Alzheimer's disease. Neurotox Res. 2013; 24:407–459. [PubMed: 23820984]

De Felice FG, Ferreira ST. Inflammation, defective insulin signaling, and mitochondrial dysfunction as common molecular denominators connecting type 2 diabetes to Alzheimer disease. Diabetes. 2014; 63:2262–2272. [PubMed: 24931033]

Duan R, Zhu L, Liu TC, Li Y, Liu J, Jiao J, Xu X, Yao L, Liu S. Light emitting diode irradiation protect against the amyloid beta 25–35 induced apoptosis of PC12 cell in vitro. Lasers Surg Med. 2003; 33:199–203. [PubMed: 12949950]

Farfara D, Tuby H, Trudler D, Doron-Mandel E, Maltz L, Vassar RJ, Frenkel D, Oron U. Low-level laser therapy ameliorates disease progression in a mouse model of Alzheimer's disease. J Mol Neurosci. 2015; 55:430–436. [PubMed: 24994540]

Farivar S, Malekshahabi T, Shiari R. Biological effects of low level laser therapy. J Lasers Med Sci. 2014; 5:58–62. [PubMed: 25653800]

Fjell AM, McEvoy L, Holland D, Dale AM, Walhovd KB. Alzheimer's Disease Neuroimaging Initiative. What is normal in normal aging? Effects of aging, amyloid and Alzheimer's disease on the cerebral cortex and the hippocampus. Prog Neurobiol. 2014; 117:20–40. [PubMed: 24548606]

Freund-Levi Y, Vedin I, Hjorth E, Basun H, Faxen Irving G, Schultzberg M, Eriksdotter M, Palmblad J, Vessby B, Wahlund LO, Cederholm T, Basu S. Effects of supplementation with omega-3 fatty acids on oxidative stress and inflammation in patients with Alzheimer's disease: the OmegAD study. J Alzheimers Dis. 2014; 42:823–831. [PubMed: 24934544]

Galluzzi L, Blomgren K, Kroemer G. Mitochondrial membrane per-meabilization in neuronal injury. Nat Rev Neurosci. 2009; 10:481–494. [PubMed: 19543220]

Gan SD, Patel KR. Enzyme immunoassay and enzyme-linked immunosorbent assay. J Invest Dermatol. 2013; 133:e12. [PubMed: 23949770]

Goodrich-Hunsaker NJ, Hunsaker MR, Kesner RP. The interactions and dissociations of the dorsal hippocampus subregions: how the dentate gyrus, CA3, and CA1 process spatial information. Behav Neurosci. 2008; 122:16–26. [PubMed: 18298245]

Griffin WS, Mrak RE. Interleukin-1 in the genesis and progression of and risk for development of neuronal degeneration in Alzheimer's disease. J Leukoc Biol. 2002; 72:233–238. [PubMed: 12149413]

Grimm A, Friedland K, Eckert A. Mitochondrial dysfunction: the missing link between aging and sporadic Alzheimer's disease. Biogerontology. 2016; 17:281–296. [PubMed: 26468143]

Han D, Scott EL, Dong Y, Raz L, Wang R, Zhang Q. Attenuation of mitochondrial and nuclear p38alpha signaling: a novel mechanism of estrogen neuroprotection in cerebral ischemia. Mol Cell Endocrinol. 2015; 400:21–31. [PubMed: 25462588]

He FQ, Qiu BY, Zhang XH, Li TK, Xie Q, Cui DJ, Huang XL, Gan HT. Tetrandrine attenuates spatial memory impairment and hippocampal neuroinflammation via inhibiting NF-kappaB activation in a rat model of Alzheimer's disease induced by amyloid-beta(1-42). Brain Res. 2011; 1384:89–96. [PubMed: 21300035]

Heneka MT, O'Banion MK. Inflammatory processes in Alzheimer's disease. J Neuroimmunol. 2007; 184:69–91. [PubMed: 17222916]

Huisa BN, Chen Y, Meyer BC, Tafreshi GM, Zivin JA. Incremental treatments with laser therapy augments good behavioral outcome in the rabbit small clot embolic stroke model. Lasers Med Sci. 2013; 28:1085–1089. [PubMed: 22945539]

Itoh K, Nakamura K, Iijima M, Sesaki H. Mitochondrial dynamics in neurodegeneration. Trends Cell Biol. 2013; 23:64–71. [PubMed: 23159640]

Jantaratnotai N, Ryu JK, Kim SU, McLarnon JG. Amyloid beta peptide-induced corpus callosum damage and glial activation in vivo. Neuroreport. 2003; 14:1429–1433. [PubMed: 12960758]

Johnstone DM, Moro C, Stone J, Benabid AL, Mitrofanis J. Turning on lights to stop neurodegeneration: the potential of near infrared light therapy in Alzheimer's and Parkinson's disease. Front Neurosci. 2015; 9:500. [PubMed: 26793049]

Karu T, Pyatibrat L, Kalendo G. Irradiation with He-Ne laser increases ATP level in cells cultivated in vitro. J Photochem Photobiol B. 1995; 27:219–223. [PubMed: 7769534]

Karu TI, Pyatibrat LV, Afanasyeva NI. Cellular effects of low power laser therapy can be mediated by nitric oxide. Lasers Surg Med. 2005; 36:307–314. [PubMed: 15739174]

Keller JN, Kindy MS, Holtsberg FW, St Clair DK, Yen HC, Germeyer A, Steiner SM, Bruce-Keller AJ, Hutchins JB, Mattson MP. Mitochondrial manganese superoxide dismutase prevents neural apoptosis and reduces ischemic brain injury: suppression of peroxynitrite production, lipid peroxidation, and mitochondrial dysfunction. J Neurosci. 1998; 18:687–697. [PubMed: 9425011]

Kim I, Rodriguez-Enriquez S, Lemasters JJ. Selective degradation of mitochondria by mitophagy. Arch Biochem Biophys. 2007; 462:245–253. [PubMed: 17475204]

Kitagawa K, Matsumoto M, Niinobe M, Mikoshiba K, Hata R, Ueda H, Handa N, Fukunaga R, Isaka Y, Kimura K. Microtubule-associated protein 2 as a sensitive marker for cerebral ischemic damage–immunohistochemical investigation of dendritic damage. Neuroscience. 1989; 31:401–411. [PubMed: 2797444]

Knott AB, Perkins G, Schwarzenbacher R, Bossy-Wetzel E. Mitochondrial fragmentation in neurodegeneration. Nat Rev Neurosci. 2008; 9:505–518. [PubMed: 18568013]

Kraft LJ, Kenworthy AK. Imaging protein complex formation in the auto-phagy pathway: analysis of the interaction of LC3 and Atg4B(C74A) in live cells using Forster resonance energy transfer and fluorescence recovery after photobleaching. J Biomed Opt. 2012; 17:011008. [PubMed: 22352642]

Leger M, Quiedeville A, Bouet V, Haelewyn B, Boulouard M, Schumann-Bard P, Freret T. Object recognition test in mice. Nat Protoc. 2013; 8:2531–2537. [PubMed: 24263092]

Lu Q, Tucker D, Dong Y, Zhao N, Zhang Q. Neuroprotective and functional improvement effects of methylene blue in global cerebral ischemia. Mol Neurobiol. 2016; 53:5344–5355. [PubMed: 26433378]

Ludwig B, Bender E, Arnold S, Huttemann M, Lee I, Kadenbach B. Cytochrome C oxidase and the regulation of oxidative phosphorylation. Chembiochem. 2001; 2:392–403. [PubMed: 11828469]

Martins RN, Harper CG, Stokes GB, Masters CL. Increased cerebral glucose-6-phosphate dehydrogenase activity in Alzheimer's disease may reflect oxidative stress. J Neurochem. 1986; 46:1042–1045. [PubMed: 3950618]

McGeer PL, McGeer EG. The inflammatory response system of brain: implications for therapy of Alzheimer and other neurodegenerative diseases. Brain Res Brain Res Rev. 1995; 21:195–218. [PubMed: 8866675]

McGeer PL, McGeer EG. Inflammation, autotoxicity and Alzheimer disease. Neurobiol Aging. 2001; 22:799–809. [PubMed: 11754986]

Meng C, He Z, Xing D. Low-level laser therapy rescues dendrite atrophy via upregulating BDNF expression: implications for Alzheimer's disease. J Neurosci. 2013; 33:13505–13517. [PubMed: 23946409]

Moreira PI, Carvalho C, Zhu X, Smith MA, Perry G. Mitochondrial dysfunction is a trigger of Alzheimer's disease pathophysiology. Biochim Biophys Acta. 2010; 1802:2–10. [PubMed: 19853658]

Moreira PI, Duarte AI, Santos MS, Rego AC, Oliveira CR. An integrative view of the role of oxidative stress, mitochondria and insulin in Alzheimer's disease. J Alzheimers Dis. 2009; 16:741–761. [PubMed: 19387110]

Muili KA, Gopalakrishnan S, Meyer SL, Eells JT, Lyons JA. Amelioration of experimental autoimmune encephalomyelitis in C57BL/6 mice by photo-biomodulation induced by 670 nm light. PLoS One. 2012; 7:e30655. [PubMed: 22292010]

Mutisya EM, Bowling AC, Beal MF. Cortical cytochrome oxidase activity is reduced in Alzheimer's disease. J Neurochem. 1994; 63:2179–2184. [PubMed: 7964738]

Palmer CS, Elgass KD, Parton RG, Osellame LD, Stojanovski D, Ryan MT. Adaptor proteins MiD49 and MiD51 can act independently of Mff and Fis1 in Drp1 recruitment and are specific for mitochondrial fission. J Biol Chem. 2013; 288:27584–27593. [PubMed: 23921378]

Parker WD Jr, Filley CM, Parks JK. Cytochrome oxidase deficiency in Alzheimer's disease. Neurology. 1990; 40:1302–1303. [PubMed: 2166249]

Parker WD Jr, Parks JK. Cytochrome c oxidase in Alzheimer's disease brain: purification and characterization. Neurology. 1995; 45:482–486. [PubMed: 7898701]

Pastore D, Greco M, Petragallo VA, Passarella S. Increase in <–H+/e− ratio of the cytochrome c oxidase reaction in mitochondria irradiated with helium-neon laser. Biochem Mol Biol Int. 1994; 34:817–826. [PubMed: 7866309]

Pettegrew JW, Panchalingam K, Klunk WE, McClure RJ, Muenz LR. Alterations of cerebral metabolism in probable Alzheimer's disease: a preliminary study. Neurobiol Aging. 1994; 15:117–132. [PubMed: 8159258]

Plass CA, Loew HG, Podesser BK, Prusa AM. Light-induced vasodilation of coronary arteries and its possible clinical implication. Ann Thorac Surg. 2012; 93:1181–1186. [PubMed: 22381453]

Qin L, Liu Y, Cooper C, Liu B, Wilson B, Hong JS. Microglia enhance beta-amyloid peptide-induced toxicity in cortical and mesencephalic neurons by producing reactive oxygen species. J Neurochem. 2002; 83:973–983. [PubMed: 12421370]

Ryu JK, Franciosi S, Sattayaprasert P, Kim SU, McLarnon JG. Minocycline inhibits neuronal death and glial activation induced by beta-amyloid peptide in rat hippocampus. Glia. 2004; 48:85–90. [PubMed: 15326618]

Sachdeva AK, Chopra K. Lycopene abrogates Abeta(1-42)–mediated neuroinflammatory cascade in an experimental model of Alzheimer's disease. J Nutr Biochem. 2015; 26:736–744. [PubMed: 25869595]

Sareddy GR, Zhang Q, Wang R, Scott E, Zou Y, O'Connor JC, Chen Y, Dong Y, Vadlamudi RK, Brann D. Proline-, glutamic acid-, and leucine-rich protein 1 mediates estrogen rapid signaling and neuroprotection in the brain. Proc Natl Acad Sci U S A. 2015; 112:E6673–E6682. [PubMed: 26627258]

Satou T, Cummings BJ, Cotman CW. Immunoreactivity for Bcl-2 protein within neurons in the Alzheimer's disease brain increases with disease severity. Brain Res. 1995; 697:35–43. [PubMed: 8593592]

Selkoe DJ. Cell biology of protein misfolding: the examples of Alzheimer's and Parkinson's diseases. Nat Cell Biol. 2004; 6:1054–1061. [PubMed: 15516999]

Serrano-Pozo A, Frosch MP, Masliah E, Hyman BT. Neuropathological alterations in Alzheimer disease. Cold Spring Harb Perspect Med. 2011; 1:a006189. [PubMed: 22229116]

Silveira PC, Silva LA, Fraga DB, Freitas TP, Streck EL, Pinho R. Evaluation of mitochondrial respiratory chain activity in muscle healing by low-level laser therapy. J Photochem Photobiol B. 2009; 95:89–92. [PubMed: 19232497]

Simonian NA, Coyle JT. Oxidative stress in neurodegenerative diseases. Annu Rev Pharmacol Toxicol. 1996; 36:83–106. [PubMed: 8725383]

Song S, Zhou F, Chen WR. Low-level laser therapy regulates microglial function through Src-mediated signaling pathways: implications for neurodegenerative diseases. J Neuroinflammation. 2012; 9:219. [PubMed: 22989325]

Souza NH, Ferrari RA, Silva DF, Nunes FD, Bussadori SK, Fernandes KP. Effect of low-level laser therapy on the modulation of the mitochondrial activity of macrophages. Braz J Phys Ther. 2014; 18:308–314. [PubMed: 25076002]

Steardo L Jr, Bronzuoli MR, Iacomino A, Esposito G, Steardo L, Scuderi C. Does neuroinflammation turn on the flame in Alzheimer's disease? Focus on astrocytes. Front Neurosci. 2015; 9:259. [PubMed: 26283900]

Sullivan PG, Brown MR. Mitochondrial aging and dysfunction in Alzheimer's disease. Prog Neuropsychopharmacol Biol Psychiatry. 2005; 29:407–410. [PubMed: 15795049]

Terni B, Boada J, Portero-Otin M, Pamplona R, Ferrer I. Mitochondrial ATP-synthase in the entorhinal cortex is a target of oxidative stress at stages I/II of Alzheimer's disease pathology. Brain Pathol. 2010; 20:222–233. [PubMed: 19298596]

Tu J, Zhang X, Zhu Y, Dai Y, Li N, Yang F, Zhang Q, Brann DW, Wang R. Cell-permeable peptide targeting the Nrf2-Keap1 interaction: a potential novel therapy for global cerebral ischemia. J Neurosci. 2015; 35:14727–14739. [PubMed: 26538645]

Urrutia PJ, Mena NP, Nunez MT. The interplay between iron accumulation, mitochondrial dysfunction, and inflammation during the execution step of neurodegenerative disorders. Front Pharmacol. 2014; 5:38. [PubMed: 24653700]

Verkhratsky A, Zorec R, Rodriguez JJ, Parpura V. Astroglia dynamics in ageing and Alzheimer's disease. Curr Opin Pharmacol. 2016; 26:74–79. [PubMed: 26515274]

von Bernhardi R, Eugenin-von Bernhardi L, Eugenin J. Microglial cell dys-regulation in brain aging and neurodegeneration. Front Aging Neurosci. 2015; 7:124. [PubMed: 26257642]

Wan H, Aggleton JP, Brown MW. Different contributions of the hippocampus and perirhinal cortex to recognition memory. J Neurosci. 1999; 19:1142–1148. [PubMed: 9920675]

Wang X, Wang W, Li L, Perry G, Lee HG, Zhu X. Oxidative stress and mitochondrial dysfunction in Alzheimer's disease. Biochim Biophys Acta. 2014; 1842:1240–1247. [PubMed: 24189435]

Wilkins HM, Carl SM, Weber SG, Ramanujan SA, Festoff BW, Linseman DA, Swerdlow RH. Mitochondrial lysates induce inflammation and Alzheimer's disease-relevant changes in microglial and neuronal cells. J Alzheimers Dis. 2015; 45:305–318. [PubMed: 25537010]

Witte ME, Geurts JJ, de Vries HE, van der Valk P, van Horssen J. Mitochondrial dysfunction: a potential link between neuroinflammation and neurodegeneration? Mitochondrion. 2010; 10:411–418. [PubMed: 20573557]

Xu Z, Guo X, Yang Y, Tucker D, Lu Y, Xin N, Zhang G, Yang L, Li J, Du X, Zhang Q, Xu X. Low-level laser irradiation improves depression-like behaviors in mice. Mol Neurobiol. 2016

Xuan W, Vatansever F, Huang L, Hamblin MR. Transcranial low-level laser therapy enhances learning, memory, and neuroprogenitor cells after traumatic brain injury in mice. J Biomed Opt. 2014; 19:108003. [PubMed: 25292167]

Yang X, Askarova S, Sheng W, Chen JK, Sun AY, Sun GY, Yao G, Lee JC. Low energy laser light (632.8 nm) suppresses amyloid-beta peptide-induced oxidative and inflammatory responses in astrocytes. Neuroscience. 2010; 171:859–868. [PubMed: 20884337]

Ying R, Liang HL, Whelan HT, Eells JT, Wong-Riley MT. Pretreatment with near-infrared light via light-emitting diode provides added benefit against rotenone- and MPP+-induced neurotoxicity. Brain Res. 2008; 1243:167–173. [PubMed: 18848925]

Zhang F, Jiang L. Neuroinflammation in Alzheimer's disease. Neuropsychiatr Dis Treat. 2015; 11:243–256. [PubMed: 25673992]

Zhang QG, Raz L, Wang R, Han D, De Sevilla L, Yang F, Vadlamudi RK, Brann DW. Estrogen attenuates ischemic oxidative damage via an estrogen receptor alpha-mediated inhibition of NADPH oxidase activation. J Neurosci. 2009; 29:13823–13836. [PubMed: 19889994]

Zhang QG, Wang RM, Scott E, Han D, Dong Y, Tu JY, Yang F, Reddy Sareddy G, Vadlamudi RK, Brann DW. Hypersensitivity of the hippocampal CA3 region to stress-induced neurodegeneration and amyloidogenesis in a rat model of surgical menopause. Brain. 2013; 136:1432–1445. [PubMed: 23474850]

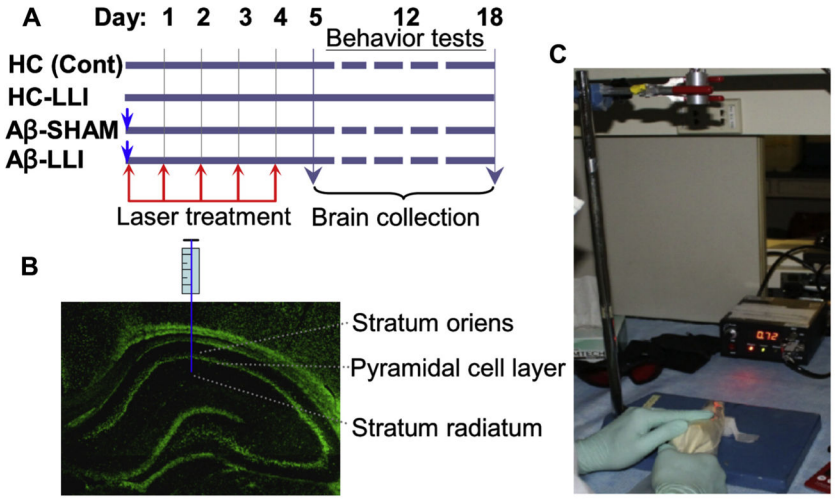

Fig. 1.

Schematic diagram of the experimental protocols. (A) Animals were randomly divided into 4 groups. Group I, healthy animals that received hippocampal vehicle infusions (HC or control). Group II, healthy animals that received LLI (HC-LLI). Group III, animals that received Aβ (1–42) infusions plus sham LLI (Aβ-SHAM, laser power was not turned on), Group IV, animals that received hippocampal Aβ (1–42) infusions plus LLI (Aβ-LLI). As shown in the figure, 2-minute daily LLI treatment was initiated 3 hours after Aβ injection for 5 consecutive days, and behavior tests were performed during days 12–18 after Aβ injection, and the brains were collected at day 6 and 18 for immunohistochemistry, Western blotting, histology, and biochemical analyses. (B) Diagram showing the intrahippocampus injection site. (C) Diagram showing laser kit and laser treatment presentation. Abbreviations: Aβ, beta amyloid; LLI, low-level laser irradiation.

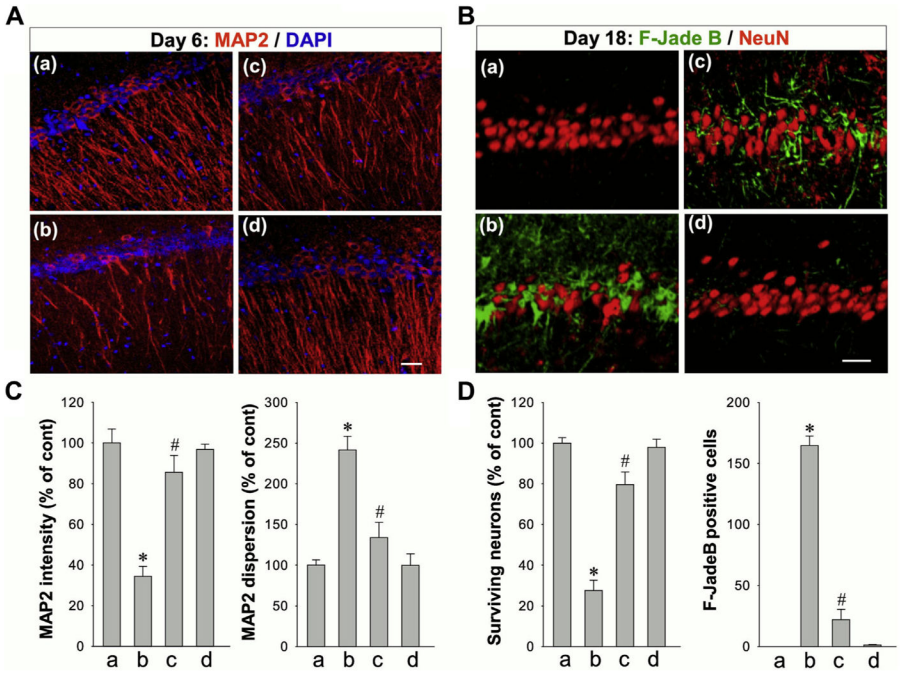

Fig. 2.

Effects of LLI on Aβ-induced neuronal injury in hippocampus CA1 region at early and late stages after Aβ (1–42) hippocampal infusion. (A) Typical staining of MAP2 (red) in healthy control animals (a: HC), animals at day 6 after Aβ (1–42) infusions without LLI (b: Aβ-SHAM) or with LLI (c: Aβ-LLI) or after scrambled Aβ (1–42) (d) infusions into the CA1 region of the hippocampus. Nuclei were counterstained with DAPI (blue). Dendrite dispersion was analyzed by using ImageJ software. Note that Aβ-induced early dendrites damage, revealed by poor dendrites morphology and increased dispersion, was reversed by LLI treatment. (B) Typical staining of F-Jade B and NeuN in control rats (a), rats at day 18 after infusion with Aβ (b: without LLI; c: with LLI) or scrambled Aβ (d) into the CA1 region of the hippocampus. Note that the neurodegeneration at the late stage was significantly attenuated by LLI. (C, D) Quantitative analyses of MAP2 intensity and dispersion in hippocampal CA1 stratum radiatum, and the numbers of surviving neurons and F-Jade B positive neurons in hippocampal pyramidal layer. $^{*}p < 0.05$ versus control group, $^{\#}p < 0.05$ versus Aβ-treated group without LLI. Data are presented as means ± standard error from 5–8 rats in each group. Scale bars represent 20 μm. Abbreviations: Aβ, beta amyloid; LLI, low-level laser irradiation. (For interpretation of the references to color in this figure legend, the reader is referred to the Web version of this article.)

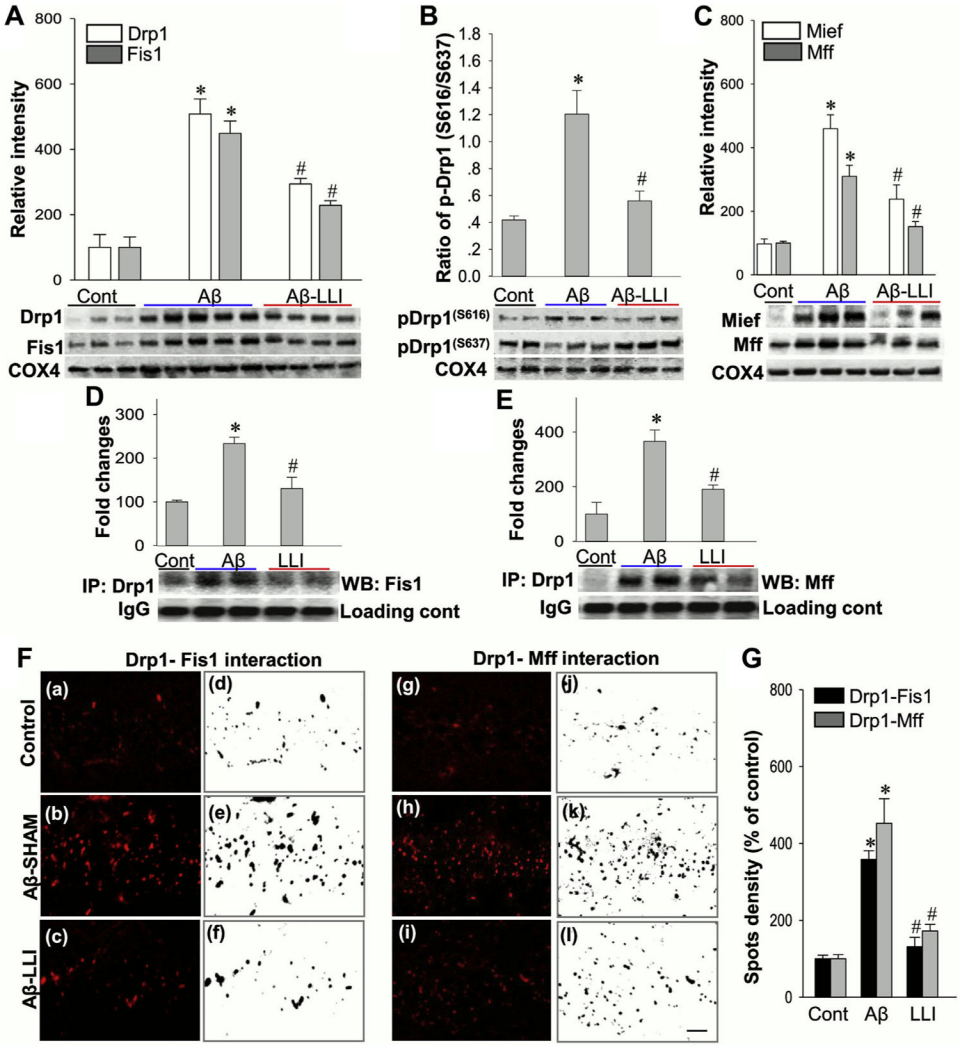

Fig. 3.

Effects of LLI on mitochondrial targeting fission proteins and the interactions. (A–C) Western blotting and quantitative analyses of mitochondrial fractions from hippocampal CA1 region were determined by the indicated antibodies to mitochondrial targeting fission proteins. COX4 was used as loading control for the mitochondrial protein. (D and E) Mitochondrial protein samples were examined by IP with anti-Drp1 antibody and then separately Western blotted with anti-Fis1 or anti-Mff antibody. (F and G) Duo-Link II in situ PLA immunoassay and quantitative analyses of the Drp1-Fis1 and Drp1-Mff interactions in the hippocampal CA1 regions 6 days after Aβ infusion (a–l). Red spots representing the interactions were converted to black images using NIH ImageJ software for better clarity and analyses. Values are shown as means ± standard error from 4 to 5 independent animals per group. $^{*}p < 0.05$ versus normal control group, $^{\#}p < 0.05$ versus Aβ-treated group without LLI. Scale bar = 10 μm. Abbreviations: Aβ, beta amyloid; IP, immunoprecipitation; LLI, low-level laser irradiation; PLA, proximity ligation assay. (For interpretation of the references to color in this figure legend, the reader is referred to the Web version of this article.)

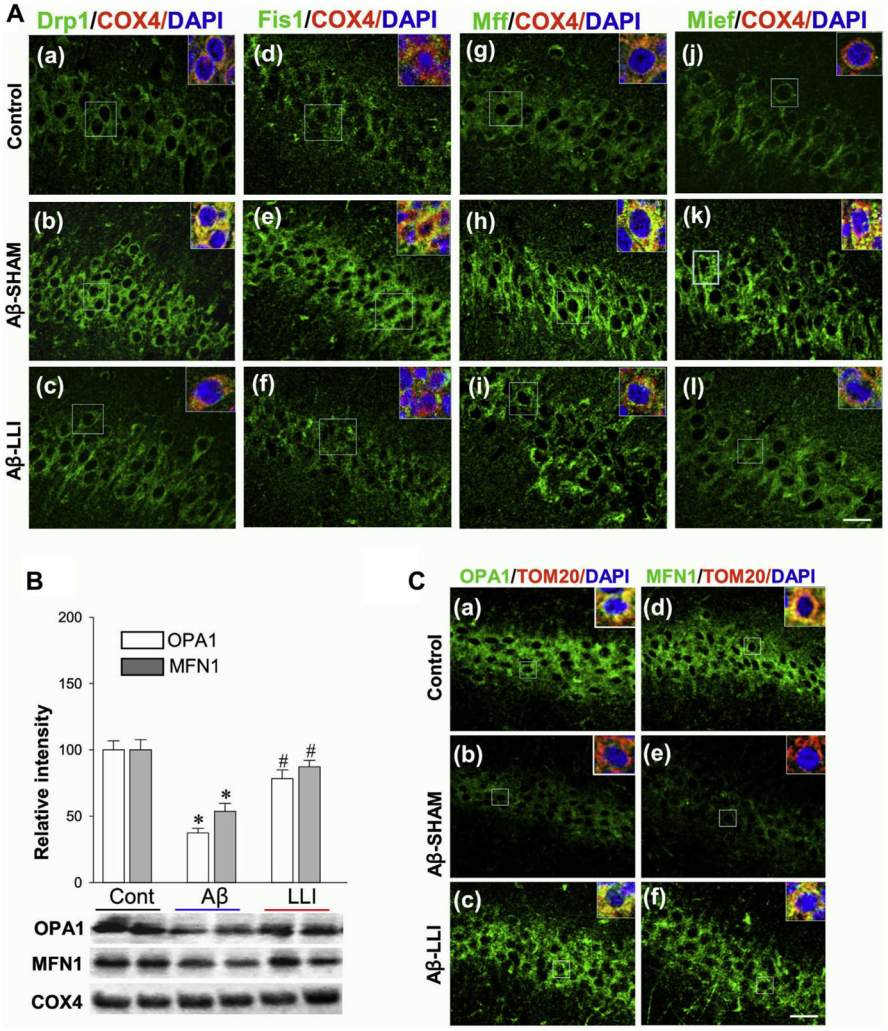

Fig. 4.

LLI suppresses the expression of mitochondrial fission proteins and preserves mitochondrial fusion proteins 6 days following Aβ injection. (A) Representative triple-labeling confocal microscopy images showing staining of mitochondrial fission proteins Drp1, Fis1, Mff, and Mief 6 days after Aβ injection (green, a–l). Insets are zooms of the boxed areas showing the mitochondrial (COX4, red) localization of fission proteins. Note the increased expression of fission proteins at early stage following Aβ insult was apparently suppressed by LLI. (B) Western blotting and quantitative analyses of mitochondrial fusion proteins OPA1 and MFN1 were performed using mitochondrial fractions from hippocampal CA1 region. Note the preservation effects of LLI on mitochondrial fusion proteins. Values are means ± standard error of determinations from each group (n = 4–5). $^{*}p < 0.05$ versus normal control group, $^{\#}p < 0.05$ versus Aβ-treated group without LLI. (C) Representative confocal microscopy images of OPA1 and MFN1 further confirmed the preservation effects of LLI on mitochondrial fusion proteins (a–f). Insets are zooms of the boxed areas showing the mitochondrial (TOM20, red) localization of fusion proteins. Nuclei were counterstained with DAPI (blue). Scale bar = 20 μm. Abbreviations: Aβ, beta amyloid; LLI, low-level laser

irradiation. (For interpretation of the references to color in this figure legend, the reader is referred to the Web version of this article.)

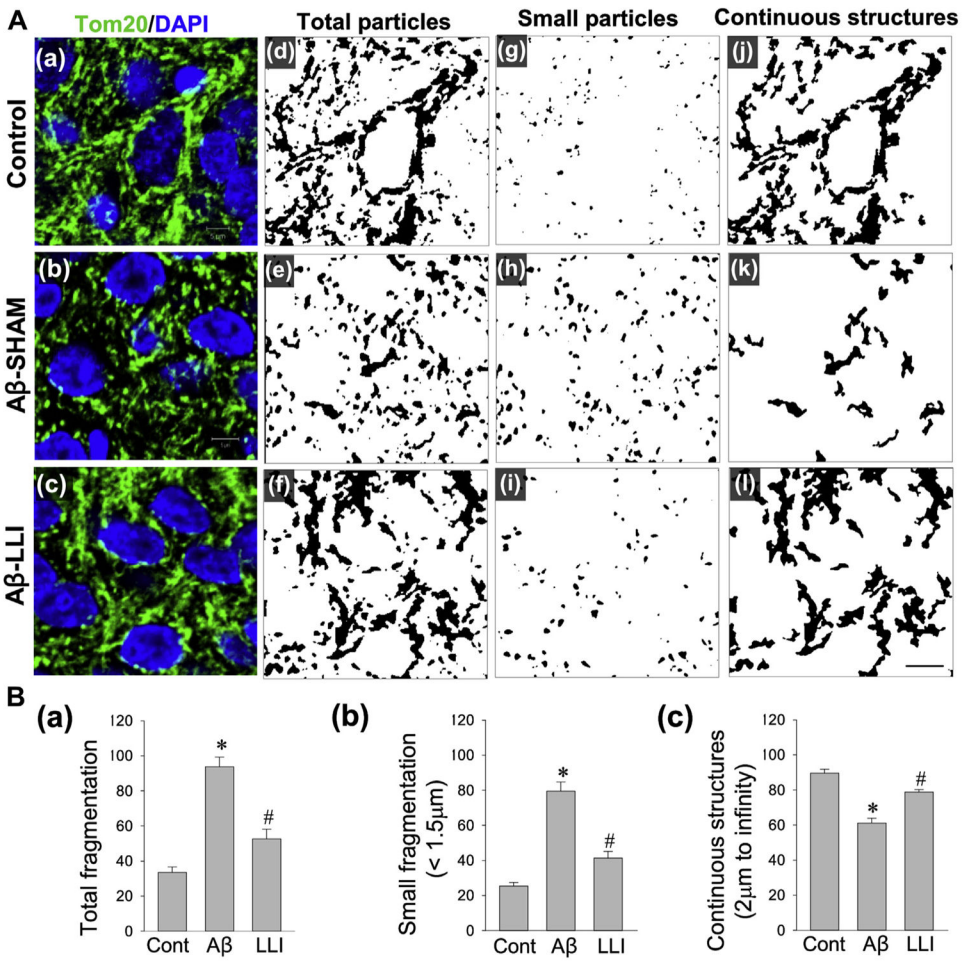

Fig. 5.

Effects of LLI on Aβ-induced changes in mitochondrial dynamics within the hippocampus CA1 neurons 6 days after Aβ infusion. (A) Representative confocal microscopy images of immunostained hippocampal CA1 pyramidal neurons with anti-Tom20 antibody (green, a–c) 6 days after Aβ infusion. Nuclei were counterstained with DAPI (blue). Acquired images of Tom20 fluorescent staining were thresholded, filtered (median, 2.0 pixels), and binarized for image views and quantitative analyses in each group. Mitochondrial segments were analyzed, using ImageJ software, for total particles (d–f), small particles (g–i, size <1.5 μm), and continuous structures (j–l, size >2 μm) to examine the effect of LLI on Aβ-induced mitochondrial fragmentation. Scale bar = 5 μm. (B) The number of total mitochondrial particles (a) and small mitochondrial particles (b) were normalized to the total mitochondrial area, respectively, to obtain the counts for total mitochondrial fragmentation and small mitochondrial fragmentation. Continuous mitochondrial structures were calculated as the percentage of the area of large particles normalized to the total mitochondrial area (c). Data are presented as means ± standard error from 5 to 7 rats in each group. $^{*}p < 0.05$ versus normal control, $^{\#}p < 0.05$ versus LLI-untreated Aβ group. Abbreviations: Aβ, beta amyloid; LLI, low-level laser irradiation. (For interpretation of the references to color in this figure legend, the reader is referred to the Web version of this article.)

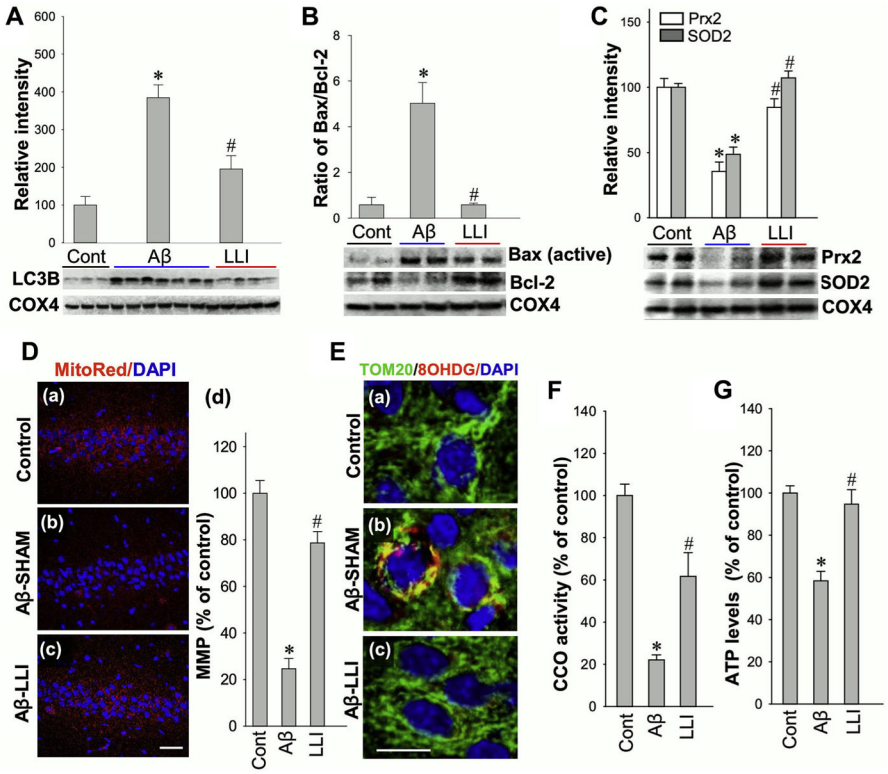

Fig. 6.

LLI attenuates mitochondrial dysfunction within the hippocampus CA1 neurons 6 days after Aβ infusion. (A–C) Western blotting and quantitative analyses of protein levels in mitochondrial fractions of hippocampal CA1 region by using the indicated antibodies. COX4 was used as loading controls for mitochondrial fractions. A ratio of Bax to Bcl-2 protein expression was further calculated. (D) Confocal microscopy analysis of MMP with fluorescent MitoTracker Red staining (a–c). The mean fluorescence (red) associated with MMP in each group was further quantified as percentage changes versus control group (d). Nuclei were counterstained with DAPI (blue). Scale bar = 50 μm. (E) Representative confocal microscopy images of immunostained hippocampal CA1 pyramidal neurons with anti-Tom20 antibody (green), anti-8OHDG (red), and DAPI (blue) 6 days after Aβ infusion (a–c). Note Aβ-induced mtDNA oxidization, merged staining (yellow) between Tom20 and 8OHDG, was reversed by LLI to a level in control group. Scale bar = 10 μm. (F and G) Cytochrome c oxidase (CCO) activity and levels of ATP production were subsequently tested using mitochondrial fractions and total protein fractions, respectively, to evaluate mitochondrial function. All the data are expressed as means ± standard error, n = 4–6 in each group. $^{*}p < 0.05$ versus control group, $^{\#}p < 0.05$ versus LLI-untreated Aβ group. Abbreviations: Aβ, beta amyloid; LLI, low-level laser irradiation; MMP, mitochondrial membrane potential; mtDNA, mitochondrial DNA. (For interpretation of the references to color in this figure legend, the reader is referred to the Web version of this article.)

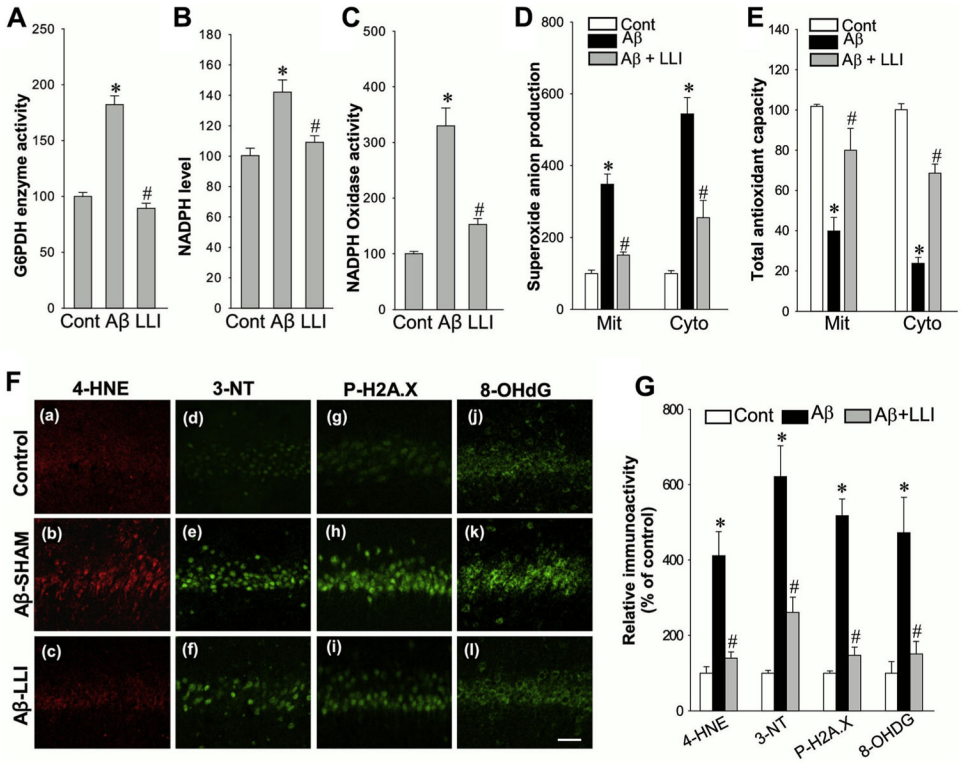

Fig. 7.

Effect of LLI on Aβ-induced G6PDH activity, NADPH oxidase activity, superoxide production and oxidative neuronal damage, and antioxidant capacity in hippocampal CA1 region. (A–E) The activities of G6PDH enzyme and NADPH oxidase, the levels of NADPH and superoxide anion production, and the antioxidant capacity were performed using the assay kits as described in detail in the Section 2. Whole-cell protein samples of hippocampal CA1 6 days after Aβ infusion were used for the detections in A–C, mitochondrial (Mit) and cytosolic (Cyto) protein samples were adopted for the assays in D and E. Data are expressed as means ± standard error (SE) from 4 to 5 animals in each group and presented as percentage changes compared with control groups. (F and G) Representative confocal microscopy images of oxidative damage markers for lipid peroxidation (4-HNE), peroxynitrite production (3-nitrotyrosine, 3-NT), DNA double-strand breaks (H2A.X Ser139), and oxidized DNA damage (8-OHdG) were taken from hippocampal CA1 region 6 days after Aβ infusion (a–l). The fluorescent intensity was quantified using ImageJ analysis software and expressed as percentage changes versus respective control group. Note that LLI strongly decreased oxidative neuronal damages 6 days after Aβ insult. Data represent means ± SE (n = 5–6 animals in each group). Scale bar: 50 μm. $^{*}p < 0.05$ versus control group, $^{\#}p < 0.05$ versus LLI-untreated Aβ group. Abbreviations: Aβ, beta amyloid; G6PDH, glucose-6-phosphate dehydrogenase; LLI, low-level laser irradiation.

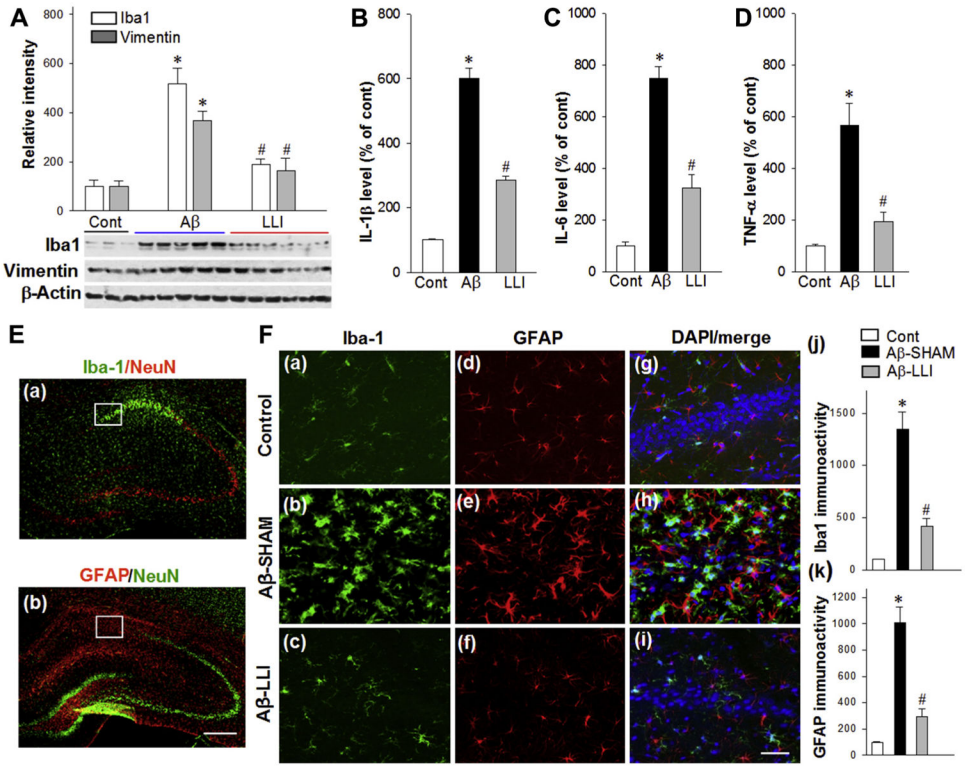

Fig. 8.

LLI inhibits Aβ-induced glial activation and proinflammatory cytokines production. (A) Western blotting and quantitative analyses of Iba1 and Vimentin, the markers for reactive microglia and reactive astrocytes, respectively, using total protein samples from hippocampal CA1 region. Note that LLI significantly suppressed Aβ-induced glial activation 6 days after Aβ injection. (B–D) ELISA assays of proinflammatory cytokines IL-1β, IL-6, and TNF-α were performed using hippocampal CA1 proteins 6 days after Aβ injection. Data are expressed as means ± standard error from 4 to 5 animals in each group and quantified as percentage changes versus normal controls. (E) Typical overview images of Iba1 (a, green) and GFAP (b, red) immunostaining showing Aβ-induced remarkable activation of microglia and astrocytes in medial hippocampal CA1 regions 18 days after Aβ injection. Brain sections were counterstained with anti-NeuN antibody. Scale bar = 500 mm. (F) Representative confocal microscopy of Iba1 (green) and GFAP (red) staining taken from medial hippocampal CA1 region at day 18 after Aβ injection (a–i). Nuclei were counterstained with DAPI (blue). Images in F are taken from the white boxed areas in the panels of E. The immunoactivity associated with Iba1 and GFAP in each group were further quantified and shown as percentage changes versus control group (j and k). The results are representative of 4–5 animals per group. Scale bar = 50 μm. $^{*}p < 0.05$ versus control group, $^{\#}p < 0.05$ versus LLI-untreated Aβ group. Abbreviations: Aβ, beta amyloid; LLI, low-level laser irradiation. (For interpretation of the references to color in this figure legend, the reader is referred to the Web version of this article.)

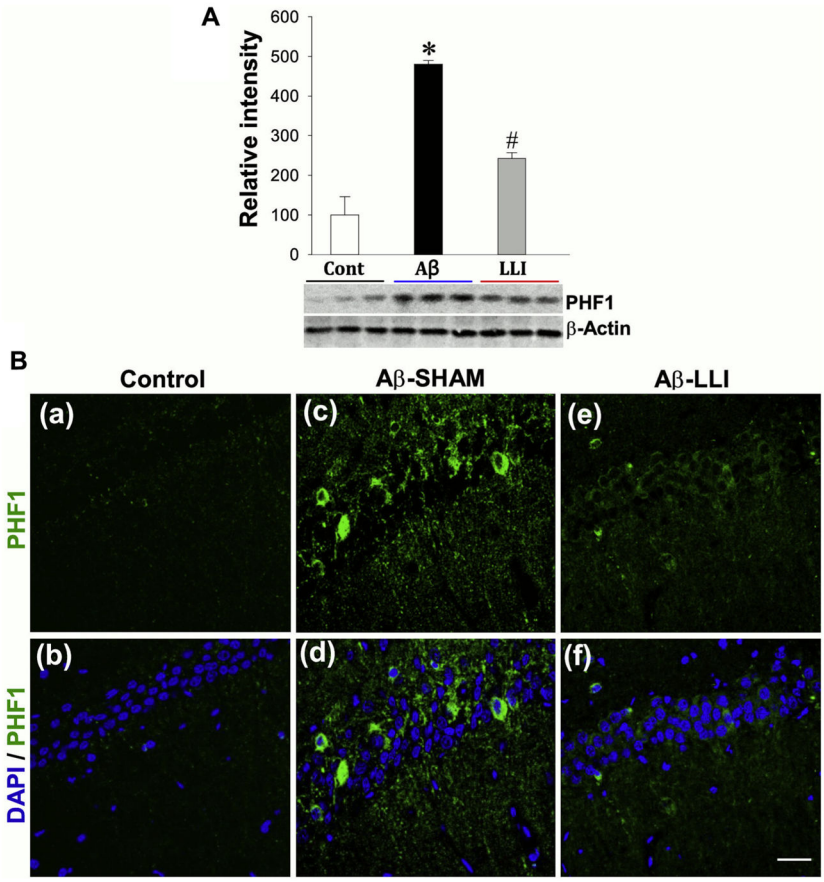

Fig. 9.

LLI suppresses the expression of hyperphosphorylated tau (PHF1) protein 6 days following Aβ injection. (A) Western blotting and quantitative analyses of PHF1 were performed using whole-cell fractions from hippocampal CA1 region. Values are means ± standard error from 4 to 5 animals in each group. $^{*}p < 0.05$ versus normal control group, $^{\#}p < 0.05$ versus LLI-untreated Aβ group. (B) Representative confocal microscopy images showing immunostaining of PHF1 protein 6 days after Aβ injection (green, a–f). Note the increased hyperphosphorylated tau protein following Aβ insult was apparently suppressed by LLI. Nuclei were counterstained with DAPI (blue). Representative images represent 5–6 animals in each group are shown. Scale bar = 20 μm. Abbreviations: Aβ, beta amyloid; LLI, low-level laser irradiation. (For interpretation of the references to color in this figure legend, the reader is referred to the Web version of this article.)

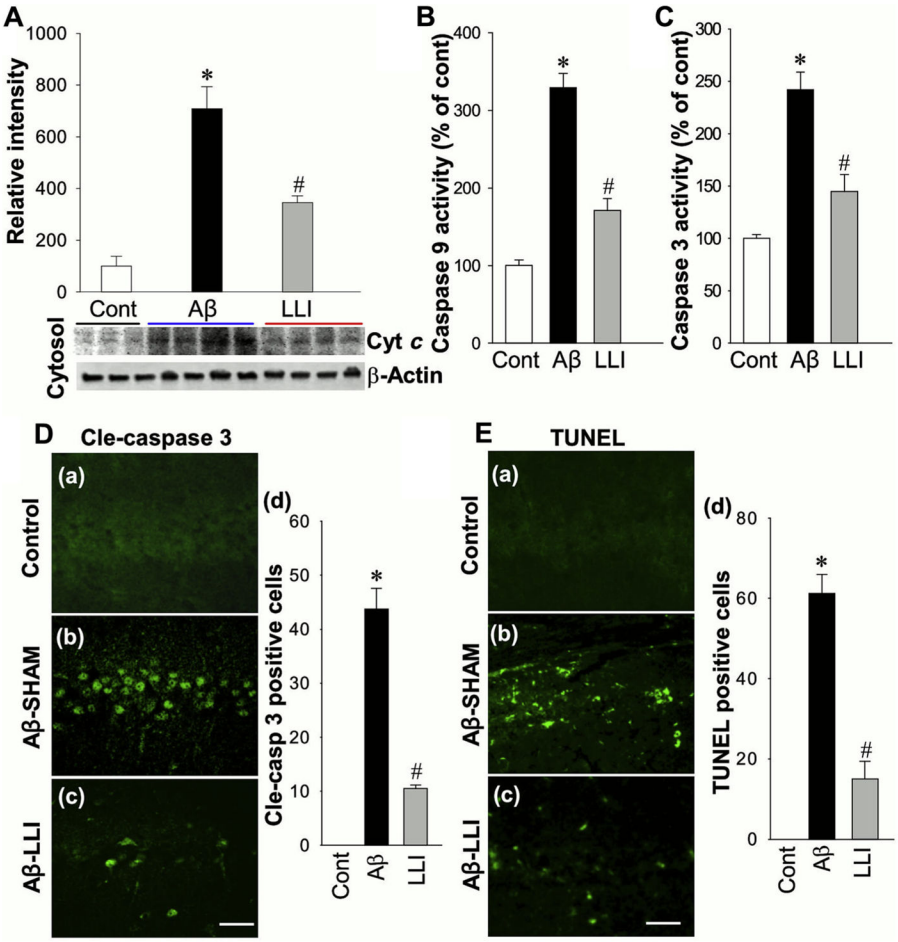

Fig. 10.

Effect of LLI on cytosolic content of cytochrome c, the activities of caspase-9 and caspase-3, and consequent apoptosis following Aβ injection. (A) Cytosolic levels of cytochrome *c* (Cyt *c*) in hippocampal CA1 region were examined by Western blotting and quantitative analyses (n = 4–5 in each group). (B and C) Caspase-9 and caspase-3 activities were measured by a fluorometric substrate assay using cytosolic proteins from CA1 region, as detailed in the Section 2. (D and E) Brain sections were subjected to immunostaining with an antibody against the active form of caspase-3, cleaved caspase-3 (Cle-caspase 3, a–c in D), as well as the TUNEL staining (a–c in E). Representative images representing 5–6 animals in each group are shown. Scale bars: 50 μm. Cell-counting studies showed significant increases in the numbers of active-caspase 3 positive cells (d in D) and TUNEL-positive cells (d in E) in Aβ-treated animals compared with the control and LLI-treated animals. The time point in A–D is day 6, and day 18 in E following Aβ injection. Values are presented as means ± standard error from each group. $^{*}p < 0.05$ versus control, $^{\#}p < 0.05$ versus LLI-untreated Aβ group. Abbreviations: Aβ, beta amyloid; LLI, low-level laser irradiation.

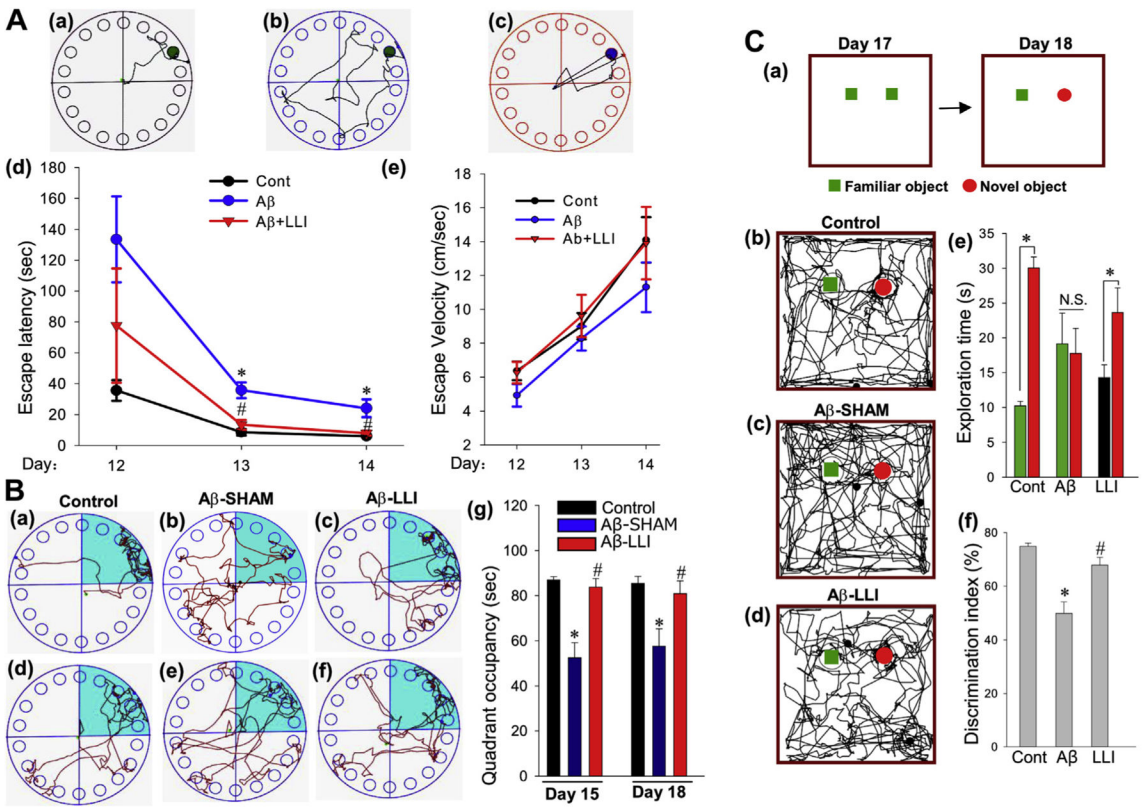

Fig. 11.

Effects of LLI on functional improvements against Aβ toxicity as measured in Barnes maze task and novel object recognition test. (A) The Barnes maze task was performed to test the spatial learning and memory ability of the indicated animals. Representative escaping traces of normal control rats (a) and rats at day 14 after infusion with Aβ (b: without LLI; c: with LLI) are shown in the up panel. The escape latency to find the black hidden box at day 12, 13, and 14 after Aβ infusion is shown in (d). Escape velocity was recorded, and statistical data are shown in (e). (B) Probe trials in the Barnes maze task were performed on day 15 and 18 after Aβ infusion, 1 day and 4 days after the last maze trials, respectively. Representative traces are presented from probe trials on day 15 (a–c) and day 18 (d–f) for the indicated animals in each group. Relative radial-quadrant occupancy (the time spent in the target radial-quadrant) was recorded and statistically analyzed. Note that Aβ-treated animals with LLI spent significantly less time to find the escape box (A, a–d) and more time in the target radial-quadrant (B, a–g) than LLI-untreated Aβ animals. (C) Five-minute novel object recognition tests at 17 and 18 days after Aβ infusion were performed to monitor the long-term recognition memory (a). Representative traces of the indicated groups to explore the familiar object and a novel object on day 18 are shown (b–d). The time spent exploring each object and the discrimination index percentage were analyzed (e and f). All the data are expressed as means ± standard error from 7 to 8 animals in each group. $^{*}p < 0.05$ versus control group or between groups (C: e), $^{\#}p < 0.05$ versus LLI-untreated Aβ group. Abbreviations: Aβ, beta amyloid; LLI, low-level laser irradiation.